Energy &
Environment Nexus

Review

Open Access

https://doi.org/10.48130/een-0025-0008

Hydrodeoxygenation of lignin derivatives on heterogeneous catalysts

Jiajun Yu, Yi Gao, Huiyan Zhang* and Rui Xiao*

Received: 19 June 2025

Revised: 11 August 2025

Accepted: 22 August 2025

Published online: 11 September 2025

Abstract

As the only abundant renewable resource containing aromatic ring structures, lignin shows tremendous potential for the production of biofuels and high-value-added chemicals. Catalytic hydrodeoxygenation (HDO) serves as a crucially important approach to convert lignin and its derived complex mixtures into valuable fuels and chemicals. However, lignin-derived compounds contain substantial amounts of oxygen-containing unstable compounds. Under high-temperature conditions, the catalysts are prone to coking and rapid deactivation. Therefore, the design of catalysts with high stable activity at low temperature and low pressure is the core of the HDO process. In recent years, numerous strategies have focused on the design of heterogeneous catalysts to enhance the reaction performance for the production of various high value-added products. This review first summarizes the possible reaction pathways for HDO of lignin-derived compounds over catalysts. Then the relationship between catalyst structure and HDO catalytic performance of reported catalysts (metal sulfides, nobel metal catalysts, non-noble catalysts) are discussed. Finally, this review presents a prospect that contributes to an in-depth understanding of the reported HDO catalysts, and provides guidance for the future design and fabrication of high-performance catalysts that can achieve precise cleavage of the target chemical bonds and selective generation of the target products.

Keywords: Solid waste resource utilization, Liquid fuels, Heterogeneous catalysts, Renewable energy and low-carbon technologies, Biomass thermal conversion

Highlights

- Reviewed the recent advances in heterogeneous catalysts for hydrodeoxygenation (HDO) of lignin derivatives.
- Summarized the possible reaction pathways for the hydrodeoxygenation (HDO) of lignin-derived compounds.
- Discussed the relationship between catalyst structure and the hydrodeoxygenation (HDO) catalytic pathway as well as performance.
- Offers guidance for the design of high-performance catalysts capable of targeted bond cleavage and selective product formation.

* Correspondence: Huiyan Zhang (hyzhang@seu.edu.cn); Rui Xiao (ruixiao@seu.edu.cn)
Full list of author information is available at the end of the article.

Graphical abstract

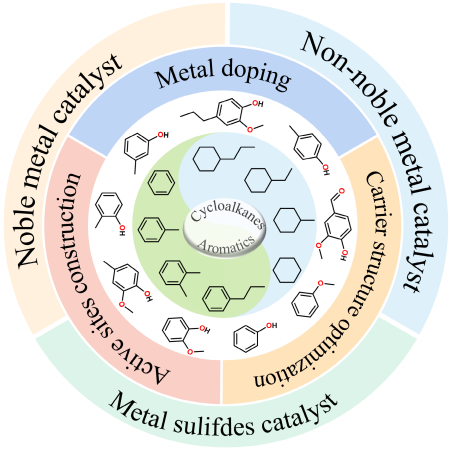

Introduction

In the global energy consumption structure, traditional fossil energy occupies a considerable proportion, exerting significant pressure on the environment and having a major impact on economic development[1,2]. Therefore, the development of both environmentally friendly and economically viable renewable energy sources is becoming increasingly attractive. As the only renewable carbon-containing resource in nature, biomass is an excellent raw material for the production of sustainable fuels and high-value chemicals. Large-scale utilization of biomass resources helps to optimize the energy structure, stabilize economic growth, and promote the sustainable development of the ecological environment[3,4]. Lignocellulosic biomass is the most abundant biomass resource in nature, consisting of cellulose (35%–50%), hemicellulose (20%–35%), and lignin (10%–25%), and has a wide range of application prospects[5]. Among them, lignin is a reticulated polymer formed by phenylpropane structural units through C–O ether bonds and C–C bonds, and is the only natural polymer with a large number of aromatic ring structures[6]. Due to its complex structure, lignin usually needs to be depolymerized at high temperatures, but its depolymerization products have low yield and poor selectivity, which represents a bottleneck for the efficient application of lignin[7–9]. Currently, cellulose and hemicellulose have been commercially utilized in the paper making, biodiesel, and bioethanol industries, while lignin has long been used as a by-product as a low-grade boiler energy[10–13]. Converting lignin to aromatic products would greatly increase the commercial viability of biorefining. Therefore, the research on depolymerizing lignin and producing high-value products is also gaining attention.

Various methods such as reductive depolymerization, pyrolysis, acidolysis, and enzymatic hydrolysis have been developed for the utilization of lignin to maximize its depolymerization into monomeric aromatic compounds[9,14,15]. The products of lignin depolymerization are usually called lignin-derived bio-oils, which are mainly composed of phenolic monomers (phenol, guaiacol, and eugenol, etc.), dimers, and oligomers (Fig. 1)[16]. These substrates serve as the primary feedstock for conversion into high-value-added chemical products[17]. However, lignin-derived phenolics contain abundant oxygen-containing functional groups, which are primarily bonded to aromatic rings and are challenging to eliminate[18]. This results in drawbacks including high oxygen content, low calorific value, high viscosity, and poor stability, all of which make lignin-derived oil unsuitable for direct use as fuel or as a fuel blending component[19–24]. Therefore, hydrodeoxygenation (HDO) under suitable reaction temperature and external H_2 has been considered as an efficient method for the upgrading of lignin-derived complex mixtures.

The HDO process is usually accompanied by a series of reactions, including direct deoxygenation, aromatic ring hydrogenation, dehydration, C-C hydrogenolysis ring opening, and transalkylation etc. (Fig. 2). The specific types of reactions depend on temperature, pressure, and the structure of the catalyst[25,26]. So far, researchers have mostly studied lignin-derived phenolic model compounds (guaiacol, phenol, and cresol, etc.) rather than structurally complex bio-oils[27,28]. Considering that the bond energy of C_{aryl}-OR (R: H, methyl or phenyl) is relatively higher, it is challenging to break this bond in HDO reactions[29–32]. HDO has been demonstrated to play a pivotal role in the conversion and upgrading of lignin and its derivatives. Although numerous excellent reviews have extensively summarized the current HDO reactions, there is still a need for a deeper review and discussion of the catalyst structure modulation strategies and the product selectivity of lignin-derived phenols. In this review, the adsorption models and HDO reaction pathways of lignin-derived phenols are first summarized, and then the mechanisms of the influence of different active sites in the catalysts on the HDO reaction are investigated, followed by a discussion of the relationship between catalyst structure modulation and the HDO reaction.

Reaction pathways for HDO of lignin-derived phenolic compounds

In general, the HDO reactions of lignin-derived phenolic compounds usually follow three main catalytic pathways: (a) direct C–O bond breaking (DDO); (b) aromatic ring hydrogenation (HYD); and (c) tautomerization (THD) (Fig. 3)[33]. Taking m-cresol as an example, path (a) involves breaking the carbon-oxygen bond while keeping the aromatic ring unchanged, resulting in toluene and water. However, as mentioned above, the C-O bond energy in the aromatic ring is high and it is challenging to break this bond. Path (b) first undergoes the hydrogenation of the aromatic ring to form the intermediate product methylcyclohexanone, followed by further hydrogenation and dehydration to obtain methylcyclohexanol, ultimately producing the cycloalkane product methylcyclohexane. Similar to path (b), path (c)

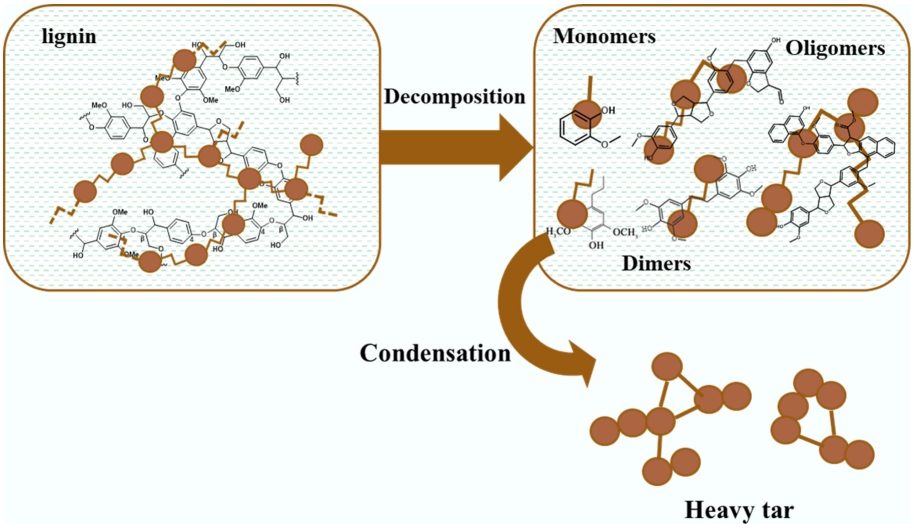

Fig. 1 Structure and properties of lignin and its depolymerization products.

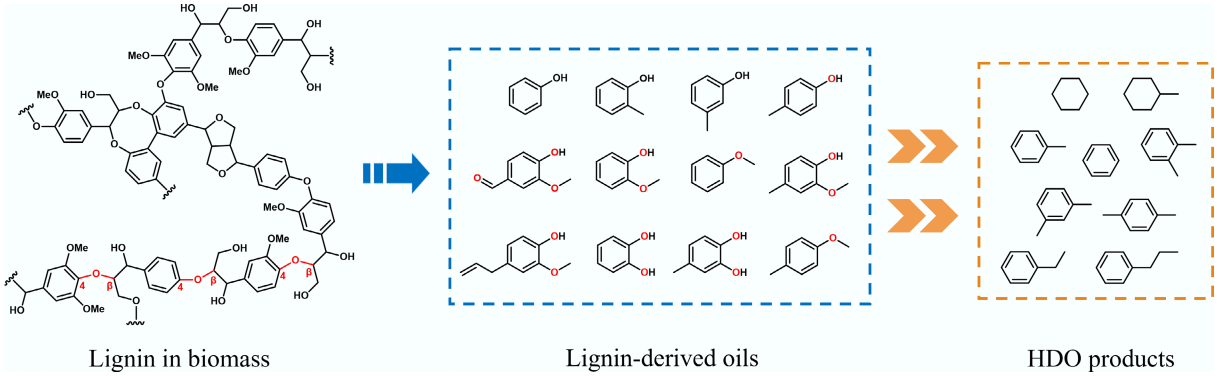

Fig. 2 Common structural features of lignin, lignin-derived oils, and HDO products.

also undergoes hydrogenation of the aromatic ring followed by dehydration, and the products contain methylcyclohexane and toluene, with the main difference being that the initial stage of path (c) undergoes reciprocal isomerization. Furthermore, in path (c), due to the poor thermodynamic conditions for the dehydrogenation of methylcyclohexene to toluene, high-pressure H_2 favors the formation of the hydrogenation product methylcyclohexane[31,34–37]. Although all three pathways ultimately result in the further conversion of phenols to aromatics or cycloalkanes, product selectivity remains highly contingent on variations in temperature, pressure, and catalyst architecture.

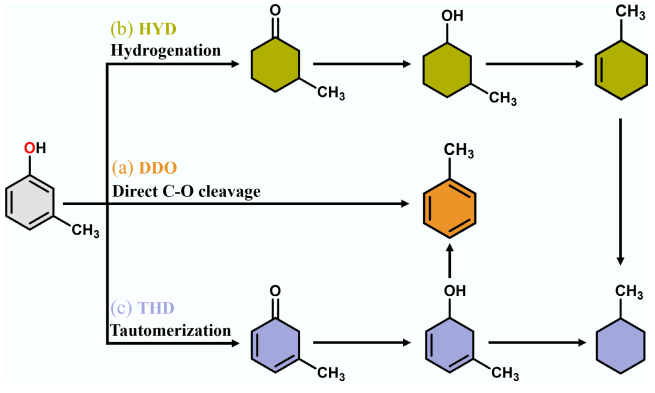

Fig. 3 Proposed conversion pathways of m-cresol HDO to toluene and methylcyclohexane.

A wide range of biomass-derived substrates has been tested in the HDO reaction. Due to their relatively simple structure, phenol is often used as a reaction substrate, and valuable products such as benzene and cyclohexane are generated during the HDO. Based on the mechanism of benzene formation from phenol HDO in a SiW_{12}-Pt/C catalyzed system at low temperature, three different C–O bond breaking paths were proposed in conjunction with density functional theory (DFT) calculations. Meanwhile, the presence of Pt also makes it possible for phenol to preferentially undergo hydrogenation to produce cyclohexanol, and the breaking of the C–O bond is the main challenge that constrains the generation of cyclohexane (Fig. 4)[38]. The conversion of cyclohexanol to cyclohexane determines the reaction rate of phenol HDO, where the synergistic interaction between Cu^0 and Cu^+ plays a crucial role in this process[39]. The Cu (111) surface is covered with hydrogen atoms, where Cu^0 adsorbed phenol forms a C–H bond, has the lowest activation barrier (105.9 kJ/mol), which is the main reaction pathway, and thus the Cu^0 site is more active in the aromatic ring hydrogenation of phenol to produce cyclohexanol. However, the dehydration of cyclohexanol on the Cu^+ species on the Cu_2O (100) surface to generate cyclohexyl intermediates is the main reaction step with an activation barrier of 90.3 kJ/mol, followed by a rapid hydrogenation to cyclohexane with an activation barrier of 88.2 kJ/mol (Fig. 5). The monometallic Cu is capable of both saturating and deoxygenating

aromatic rings. As a representative of bio-oil compounds containing C_{aryl}-O-C bonds, anisole is also frequently used as a model compound in the HDO process, where four main reaction pathways occur: hydrogenation, hydrolysis, demethylation, and transalkylation. Guaiacol is one of the most widely used phenolic model substrates, containing three distinct types of C–O bonds. As a complex model compound, guaiacol can represent lignin and its many derivatives[40,41]. In early HDO studies, guaiacol typically yielded a range of valuable chemicals including catechols, methylation products, and deoxygenation products such as phenol, benzene, cyclohexanol, and cyclohexane[42].

The study of reaction mechanisms is complicated by the increase of oxygen-containing functional groups in model compounds and the existence of more potential reaction pathways. Runnebaum et al.[43] analyzed the HDO products of Pt/γ-Al_2O_3 catalysts at 573 K and postulated possible reaction pathways for lignin-derived representative compounds (Fig. 6), including the above-mentioned guaiacol, phenol, anisole, and other reaction intermediates (cyclohexanone

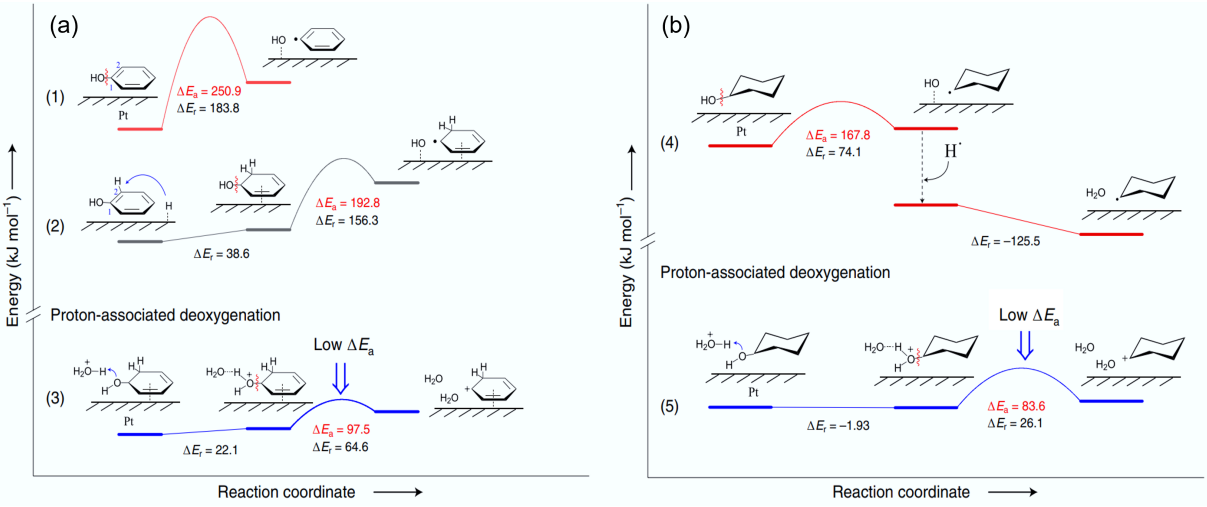

Fig. 4 Energy profiles of possible C–O bond breaking pathways for (**a**) phenol, and (**b**) cyclohexanol in HDO on the Pt (111) surface. ΔE_r: reaction energy, ΔE_a: activation energy. Reproduced with permission[38]. Copyright 2020, Springer Nature.

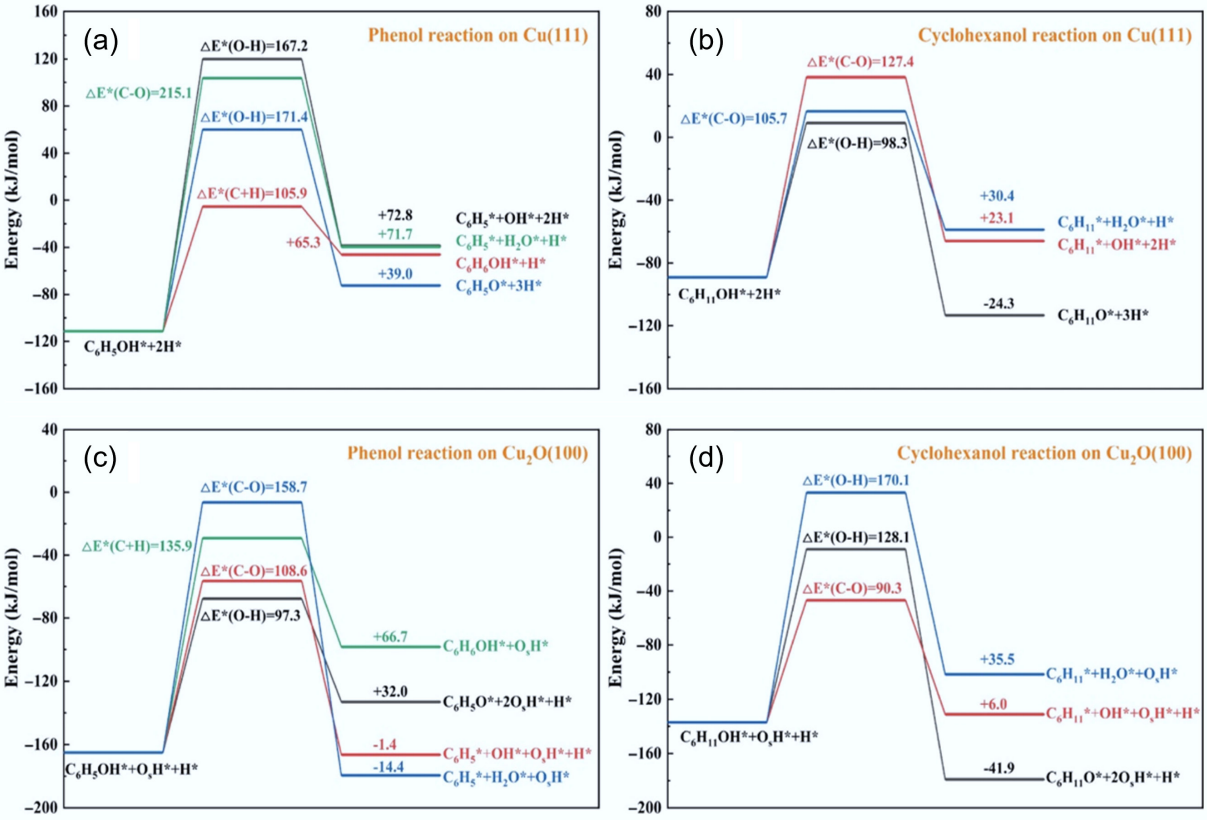

Fig. 5 (a) Phenol and (b) cyclohexanol reaction over Cu (111), and (c) Phenol and (d) cyclohexanol reaction over Cu (111) Cu_2O (100) surfaces. Reproduced with permission[39]. Copyright 2022, American Chemical Society.

and 4-methylanisole). The reaction pathway of guaiacol is more complex than those of other phenolic compounds, and its pathway contains both phenol and anisole reactions. This is mainly due to the presence of three different types of C-O bonds in guaiacol, which are also present in phenol and anisole, respectively. When one of these functional groups undergoes direct hydrogenolysis, phenol or anisole is obtained. Although the components of bio-oils are very complex and include a range of compounds containing other functional groups in addition to the derivatives mentioned above, It generally follows the above deoxidation reaction pathways and depends on the structure of the substances themselves. It is believed that this proposed reaction pathway diagram is informative for most catalysts, and it also illustrates the feasibility of choosing lignin-derived compounds as a substitute for bio-oil for the performance evaluation of HDO reactions.

Development of heterogeneous catalysts for HDO of biomass-derived compounds

The design and synthesis of catalysts featuring high activity, selectivity, and stability represent the core challenge for enhancing the efficiency of the HDO reaction. The following section Table 1 summarizes HDO catalysts reported in recent years, particularly focusing on the effects of active metal sites, acid sites, and modulation of interfacial properties on catalyst activity and hydrodeoxygenation reaction pathways of metal catalysts. Although high temperature facilitated the rate of the HDO reaction[44], coke tended to form on the surface of the catalyst at high temperature to deactivate the active sites. Besides, the catalyst itself could also be deactivated due to sintering. Therefore, research activities are focused on catalysts that significantly reduce the reaction temperature and are highly resistant to carbon deposition[32,37,45–47]. Since the HDO process has multiple reaction pathways, unique catalysts should be designed to modulate the active sites of the catalysts to generate aromatic hydrocarbons or cycloalkanes with high selectivity. This review summarizes the recent progress of metal sulfides, noble metals, and non-noble metal catalysts in HDO and the corresponding modulation strategies, including second-metal doping, active-site construction, and optimization of the carrier structure. This paper provides guidance on regulating the selectivity of the HDO reaction and delivers insights into catalytic mechanisms for the rational design of highly efficient and selective HDO catalysts toward aromatic hydrocarbons or cycloalkanes production.

Metal sulfides

Metal sulfide catalysts were initially mainly applied in hydrodesulfurization (HDS) and hydrodenitrogenation (HDN) processes in petroleum refining[68]. Due to their high hydrogenation activity, researchers also explored the performance of sulfide catalysts in the HDO of lignin-derived phenols[69]. In particular, MoS_2-based catalysts have made great progress, and with further research, an increasing

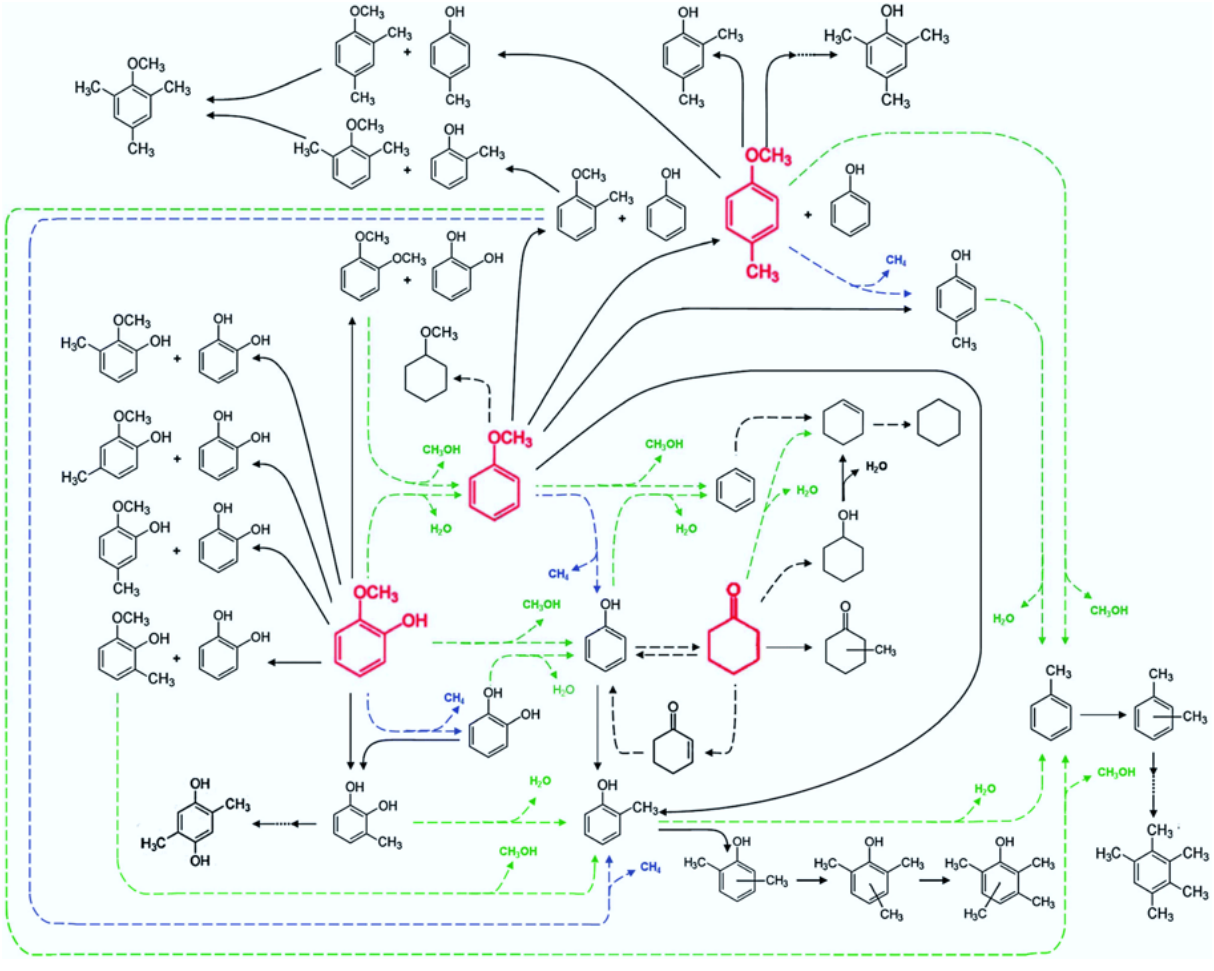

Fig. 6 Reaction pathway for the conversion of lignin-derived compounds under Pt/γ-Al_2O_3. Reproduced with permission[43]. Copyright 2012, Royal Society of Chemistry.

Table 1 HDO of lignin-derived model compounds over heterogeneous catalysts

Catalysts	Reaction conditions			Substrate	Conv. (%)	Products	Sel. (%)	Ref.
	T (°C)	P (bar)	Solvent					
$^{F}MoS_2$	300	30	decalin	p-cresol	69.6	toluene	87.2	[48]
$^{S}MoS_2$	300	30	decalin	p-cresol	98.7	toluene	83.1	[48]
Co-$^{F}MoS_2$	180	30	decalin	p-cresol	21.0	toluene	98	[48]
Co-$^{S}MoS_2$	180	30	decalin	p-cresol	97.6	toluene	98.4	[48]
CoS_2/MoS_2	220	30	dodecane	p-cresol	58.9	toluene	95.2	[49]
Co-Mo-S	220	30	dodecane	p-cresol	88.5	toluene	97.4	[49]
$Mo_{0.06}–Co_9S_8/Al_2O_3$	265	40	–	DPE	99.8	benzene	91	[50]
Pt-Mo-200	120	50	–	p-cresol	100	MCH	96.3	[51]
Pd/m-$MoO_3–P_2O_5/SiO_2$	110	10	decalin	phenol	100	cyclohexane	97.5	[52]
Pt-WO_{3-x}	230	30	n-hexane	phenol	99	cyclohexane	94.3	[53]
Ru/TNP	250	10	octane	guaiacol	99.9	cyclohexane	100	[54]
Ru/C-HPW	200	10	octane	guaiacol	100	cyclohexane	92.1	[55]
Ru@H-ZSM-5	150	50	water	phenol	60	cyclohexane	51	[56]
Pd-ZrO_2	300	1	–	m-cresol	14.7	toluene	87.9	[57]
Pd-ZrO_2	300	1	–	phenol	77	benzene	66	[58]
Pt-WO_x/C	300	36	dodecane	m-cresol	61	toluene	98	[59]
Br-Ru/C	120	5	methanol	DPE	99.8	benzene	44.7	[60]
Ni-Co-NbO_x	300	30	dodecane	guaiacol	100	cyclohexane	98.9	[61]
Fe-ZrO_2	300	40	octane	guaiacol	17.1	cyclohexane	0.4	[62]
FeNi-ZrO_2	300	40	octane	guaiacol	100	cyclohexane	89.4	[62]
Ni/SiO_2	340	40	dodecane	m-cresol	19.6	MCH	63.6	[63]
Ni/ZrO_2	340	40	dodecane	m-cresol	18.2	MCH	56.8	[63]
Ni_2P/SiO_2	340	40	dodecane	m-cresol	20.2	MCH	62.9	[63]
Ni_2P/ZrO_2	340	40	dodecane	m-cresol	20.9	MCH	74.3	[63]
Ni_2P/SiO_2	250	30	dodecane	m-cresol	94.7	MCH	96.3	[64]
$Ni_{15}Fe_5/ZrO_2$	300	20	n-hexane	p-cresol	98.1	MCH	68.7	[65]
$Ni_{15}Co_5/ZrO_2$	300	20	n-hexane	p-cresol	100	toluene	34.9	[65]
5% Ni/SiO_2	300	1	–	m-cresol	95.6	toluene	67.6	[66]
Ni-Mo/SiO_2	350	1	–	m-cresol	95	toluene	> 80	[67]

number of metal sulfide catalysts have been designed and developed to enhance the HDO reaction rate.

Molybdenum disulfide (MoS_2) is a crystal structure consisting of vertically stacked S-Mo-S layers that are held together by van der Waals forces[70,71]. Mo atoms and S atoms are arranged in a weakly interacting S-Mo-S layer through a hexagonal lattice arrangement. Each S atom is coordinated to three Mo atoms in monolayer MoS_2 (layer thickness 6.5 Å), with a standard Mo-S bond length of 2.42 Å (Fig. 7a)[70,72]. Since the sandwich structure of the S-Mo-S layer results in anisotropic crystals, researchers have proposed four MoS_2 polycrystalline types, 1T MoS_2, 1H MoS_2 (the most stable), 2H MoS_2, and 3R MoS_2[73]. Numerous experiments have confirmed that the high catalytic activity of MoS_2 mainly originates from the formation of S vacancies on its edge sites, thus exposing unsaturated ligand Mo atoms[70,74,75].

Three main structural models have been put forward to elucidate the catalytic properties of MoS_2, including the rim-edge model[78], remote control model[79], and Co-Mo-S model[77]. The Rim-edge model was first proposed by Daage et al. in the HDS reaction of dibenzothiophene(DBT), which describes a multilayer sulfide with different average stacking layers (Fig. 7b)[78]. Hydrogenation of the aromatic ring primarily took place at the rim sites on account of their higher coordinative unsaturation, whereas hydrogenolysis occurred at both the rim and edge sites. Wang et al. applied a hydrothermal method to synthesize MoS_2 catalysts with different stacking numbers[80]. It was demonstrated that increased stacking layers in catalysts led to improved DDO selectivity, while MoS_2 with fewer stacked layers exhibited a preference for the HYD pathway. The synergistic interaction between the doping of a second metal and MoS_2 can be aptly interpreted by the remote control model put forward by Delmon & Froment[79]. Their hypothesis suggested that the catalytic activity and selectivity of bimetallic MoS_2 catalysts stemmed from synergistic interactions between two coexisting phases. Specifically, the synergistic interaction between CoS_x and MoS_2 was commonly referred to as the remote-control model.

The Co-Mo-S model was first proposed by Lauritsen et al.[77], and it currently stands as the most widely accepted model in the field of HDO reactions. This model employed sulfur vacancies as active sites for selective deoxygenation, where enhanced catalytic activity and aromatic selectivity were achieved through increasing surface sulfur vacancy density[81]. It is generally believed that the addition of Co to MoS_2 can improve the HDO activity. Co atoms are located at the edge of MoS_2 and provide electrons to Mo for chemical interaction, which weakens the Mo–S bond at the Co-anchoring position and promoted the elimination of S[31]. Through combined scanning tunneling microscopy (STM), and density functional theory (DFT) studies, Topsøe's research group conducted in-depth investigations into the atomic-scale structure of Co/Ni-promoted MoS_2 nanoclusters. They determined that the Co-Mo-S phase presented a sub-hexagonal morphology, with Co atoms preferentially localized at the (1(-)010) edge featuring a 50% S coverage (Fig. 7c). According to the STM images of the Ni-Mo-S phase, type A (larger MoS_2 nanoclusters) had similar features to the Co-Mo-S phase (Fig. 7d), while type B (smaller MoS_2 nanoclusters) showed a dodecagonal shape with three different edges at the end (Fig. 7e).

Metal-doped MoS_2 catalysts are currently one of the most promising materials for HDO reactions. Doped metals like Pt and Ni with excellent hydrogen dissociation abilities tend to undergo

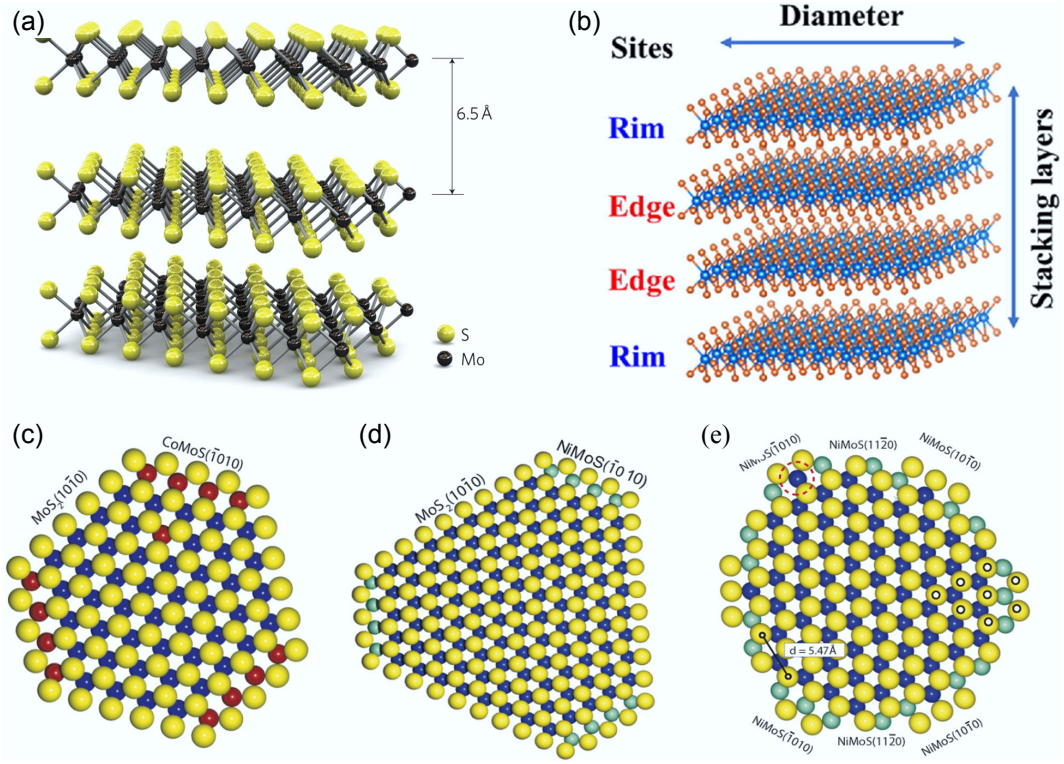

Fig. 7 (**a**) Three-dimensional model of the MoS_2 structure. Reproduced with permission[70]. Copyright 2011, Springer Nature. (**b**) Rim-edge model of an MoS_2 catalytic particle. Reproduced with permission[76]. Copyright 2023, Elsevier. Ball model of (**c**) Co–Mo–S, (**d**) type A Ni–Mo–S, (**e**) type B Ni–Mo–S. S: yellow, Mo: blue, Co: red, Ni: cyan. Reproduced with permission[77]. Copyright 2007, Elsevier.

cyclohydrogenation reactions, allowing selective preparation of cycloalkane products under mild conditions[38,82]. The noble metal Pt is highly prone to sulfidation under H_2S exposure, resulting in severe catalyst deactivation[83]. To significantly improve the activity of MoS_2, Wu et al. devised a novel metal insertion-deinsertion strategy for the synthesis of the Pt-MoS_{2-x} catalyst[51]. During the formation of Pt-MoS_{2-x}, Pt^{4+} initially undergoes partial substitution for Mo atoms in the basal plane of the 1T-phase. Subsequently, Pt is deinserted from the basal plane, yielding isolated Pt atoms and generating new edge sites on the basal plane of the 2H-phase. This process achieves activation of the inert basal plane (Fig. 8a). The extended X-ray absorption fine structure (EXAFS) results proved that Pt species existed in the form of Pt-O and Pt-Pt bonds in the Pt-Mo-200 spectrum, compared to the PtS_2 standard sample, where Pt was present as Pt-S. This indicated the cleavage of Pt–S bonds and the formation of metallic Pt nanoparticles at the edge position of the basal plane. This observation aligned with the results obtained through high-angle annular dark-field scanning transmission electron microscopy (HAADF-STEM) analysis (Fig. 8b-f). In the HDO process of p-cresol, the catalyst achieved 100% deoxygenation at a low temperature of 120 °C, and with a 96.3% yield of methylcyclohexane. Almost no S loss or deactivation was observed in the stability tests.

The incorporation of Co can alter the morphology, structure, and electron cloud density distribution of MoS_2. This modification significantly increases the number of S vacancies on the surface of the Co-Mo-S phase, leading to the formation of more active sites[76]. This led to enhanced selectivity in the conversion of lignin derivatives to aromatics, accompanied by high hydrodeoxygenation activity and outstanding stability[84,85]. In their investigation of m-cresol hydrodeoxygenation (HDO) performance, Cao et al. developed two Co-doped MoS_2 model catalysts (Fig. 9a), with the active phase structure being characterized through X-ray diffraction (XRD), scanning electron microscopy (SEM), and X-ray photoelectron spectroscopy (XPS) analyses[49]. The results demonstrated that the Co-Mo-S phase catalyst exhibited notably higher HDO activity compared to the CoS_2/MoS_2 catalyst, achieving a conversion of 88.5% and a toluene selectivity of 97.4%. The high activity of the Co-Mo-S phase was attributed to the significant weakening of the Mo–S bond, which promoted the formation of new S vacancies at the Co-Mo-S interface and improved the reaction rate and aromatic selectivity of the DDO pathway. In addition, Liu et al. synthesized a novel catalyst by dispersing Co species on a MoS_2 monolayer. They mixed the prepared MoS_2 monolayer with thiourea-based Co species to covalently bind Co atoms to sulfur vacancies on MoS_2[48]. The monolayer MoS_2-based catalysts synthesized exhibited superior activity, selectivity (99.2%), and stability towards the HDO of p-cresol compared to those prepared by the conventional methods for bulk catalysts (Fig. 9b). The performance of HDO was significantly improved owing to the generation of numerous S vacancies (Fig. 9c). This unique catalyst structure allowed the reaction temperature to be reduced to 180 °C and no S loss was detected during the catalytic process. In summary, the formation of the Co-Mo-S phase notably enhanced the HDO catalytic efficiency of MoS_2-based systems.

In situ formation of substantial water occurred during the HDO reaction. The produced water interacts readily with the active site of the Co-doped MoS_2 catalyst at elevated temperature, leading to the loss of S from the Mo active sites, and consequently causing catalyst deactivation[86,87]. Thus, a synthetic strategy of loading highly dispersed Mo on hydrotalcite-derived Co_3O_4/Al_2O_3 and subsequent sulfidation was proposed by Diao et al. to prepare the Mo-Co_9S_8/Al_2O_3 catalyst (Fig. 10a)[50]. By enclosing the active Co-Mo

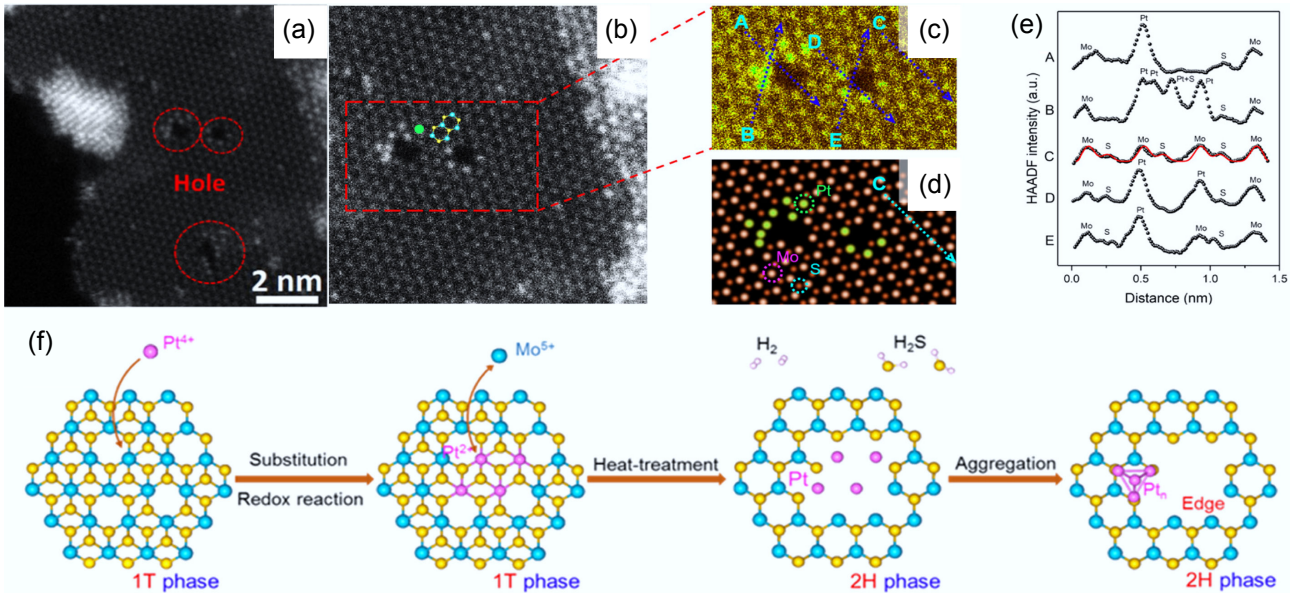

Fig. 8 (**a**) Pt-Mo-200, and (**b**), (**c**) enlarged HAADF-STEM images. (**d**) Simulated high-resolution HAADF-STEM results for Pt-Mo-200. (**e**) Measurement of the intensity profiles of the four lines labeled in (**c**) and (**d**). (**f**) Schematic of the synthesis of Pt-MoS_{2-x} catalyst. Reproduced with permission[51]. Copyright 2021, American Chemical Society.

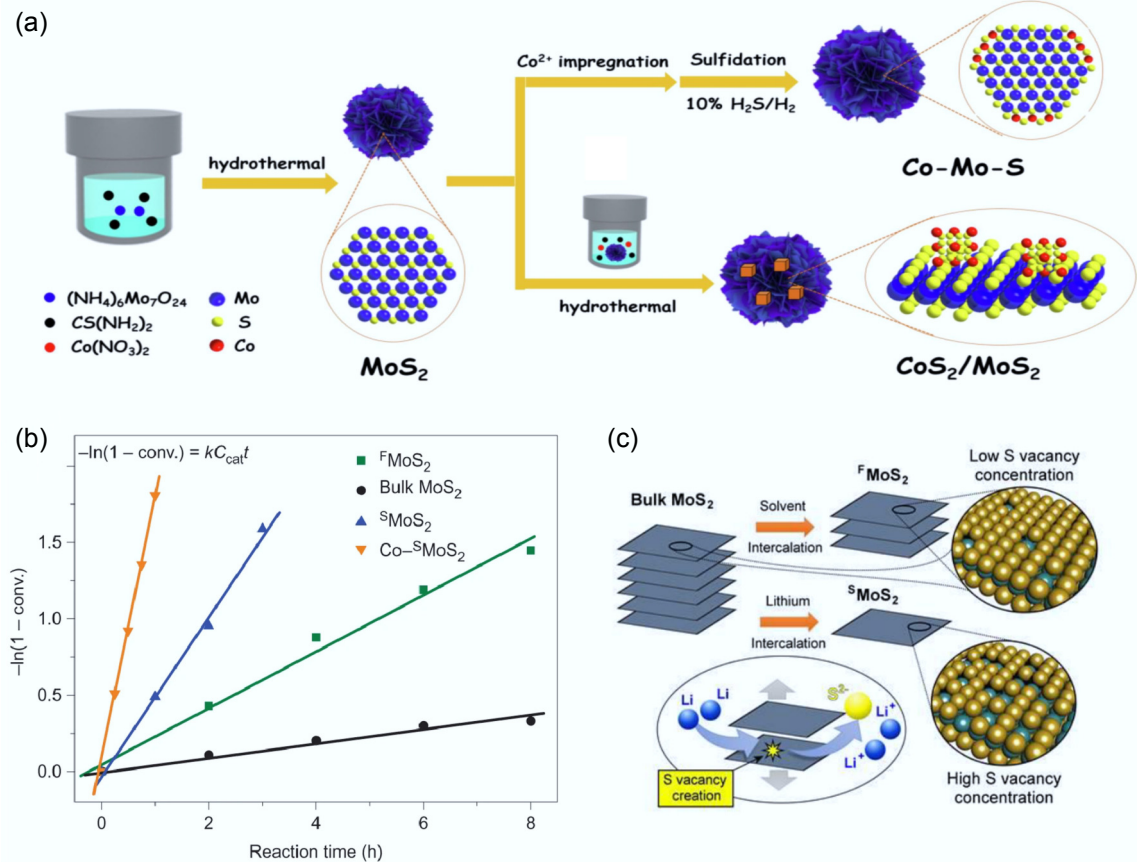

Fig. 9 (**a**) Schematic illustration of the preparation routes for Co-Mo-S and CoS_2/MoS_2 catalytic materials. Reproduced with permission[49]. Copyright 2023, Elsevier. (**b**) Kinetic study of p-cresol to toluene at 3 MPa and 300 °C, the order of activity: Co-$^{S}MoS_2$ > $^{S}MoS_2$ > $^{F}MoS_2$ > bulk MoS_2. (**c**) Physical (solvent intercalation) and chemical (Lithium intercalation) exfoliation methods of bulk MoS_2, S: yellow, Mo: green. Reproduced with permission[48]. Copyright 2017, Springer Nature.

interfacial sites in the water-absorbent rich inert Co_9S_8 species, this indirect protection approach avoided the contact between water and active sites, thus enabling the catalyst to exhibit strong resistance to water deactivation[68]. In this study, complete removal of the oxygen atom from 2.5 mmol of diphenyl ether would theoretically yield 45 mg of water. Under the same conditions, the

moderate addition of water increased the yield of aromatics. However, excessive water resulted in a competitive adsorption behavior between water and diphenyl ether, reducing the conversion and yield (Fig. 10b). From the XRD pattern of the recovered catalysts, with the increase of water, the abundant Co_9S_8 on catalyst surface was preferentially passivated and transformed into cobalt sulfate hydrate (Fig. 10c). Meanwhile, the active interface remained essentially intact, attributed to the protective role of Co_9S_8 (Fig. 10d). Stability testing of the above recovered catalysts revealed that the catalysts with cobalt sulfate hydrate as the main phase exhibited enhanced benzene yield and fully reverted to the Co_9S_8 phase at the end of the reaction (Fig. 10e,f). In addition, the anchoring effect of the Al_2O_3 matrix also made the catalyst resistant to high-temperature sintering. This highly selective and robust catalyst was capable of converting raw lignin into aromatics, even under challenging reaction conditions.

Although sulfide catalysts show high selectivity in HDO, the constant addition of H_2S/C_2S to regenerate the catalyst is required due to S loss during the reaction. At the same time, the catalysts are subject to contamination and rapid deactivation due to coke deposition. The large amount of water generated during the HDO process seriously affects the performance of the active sites, so the improvement of water resistance is a challenge that needs to be solved urgently. Decreasing the reaction temperature is currently the most stable and cost-effective strategy used to inhibit S loss, water toxicity, sintering, and carbon deposition. Nevertheless, achieving high catalytic activity in MoS_2-based systems under low-temperature conditions remain a significant scientific challenge.

Noble metal catalysts

In view of the excellent low-temperature activity and hydrogenation properties of noble metals, especially in the selectivity for cycloalkanes, noble metals have been extensively studied in HDO[88,89]. The reaction network and TOF of the corresponding steps for the hydrogenation of guaiacol on Pt (111) at atmospheric pressure to aromatic products were investigated by theoretical calculation and are shown in Fig. 11[90]. At 573 K, the production of the main product catechol was found to be at least four orders of magnitude faster than its further deoxygenation to phenol or benzene. The slow deoxygenation of guaiacol can be achieved through decarbonylation, hydrogenation of the benzene ring, and cleavage of the -OH bond. In the absence of an activated aromatic ring, the deoxygenation rate is reduced by at least five orders of magnitude.

Compared with monometallic catalysts, the incorporation of a second metal can alter the d-band electron density and surface morphology of the primary metal. Due to the synergistic interaction between the two metals, bimetallic catalysts show good activity, selectivity, and stability for C–O bond breaking in HDO[91–97]. It has further been observed that bimetallic catalysts efficiently suppress polymerization, condensation, and carbon deposition throughout the catalytic process[33,52,61,66]. For instance, literature reports indicate that the high activity of Pd-Fe bimetallic catalysts in HDO stems from the interaction between Pd and Fe, which shifts the d-band center of Pd[98,99]. The incorporation of Fe altered the electronic configuration of Pd, resulting in attenuated adsorption of both reaction intermediates and final products. In addition, the presence of Pd prevented the deactivation of the catalyst due to Fe oxidation, thus preserving the formation of metallic Fe in the HDO process. The Pt-Mo bimetallic catalyst exhibits high selectivity for aromatic hydrocarbons in the HDO of lignin derivatives (Fig. 12a). The addition of Pt alters the structure of Mo, enhancing the hydrogen decomposition and the hydrogenation desorption of intermediates. The presence of Pt also promotes the alkylation reaction, retaining more hydrocarbon elements in the liquid product (Fig. 12b). Moreover, the presence of oxygen-rich vacancies in TiO_2 enhances the adsorption of oxygen-containing substrates, preventing catalyst deactivation due to the activity of Mo (Fig. 12c, d)[100].

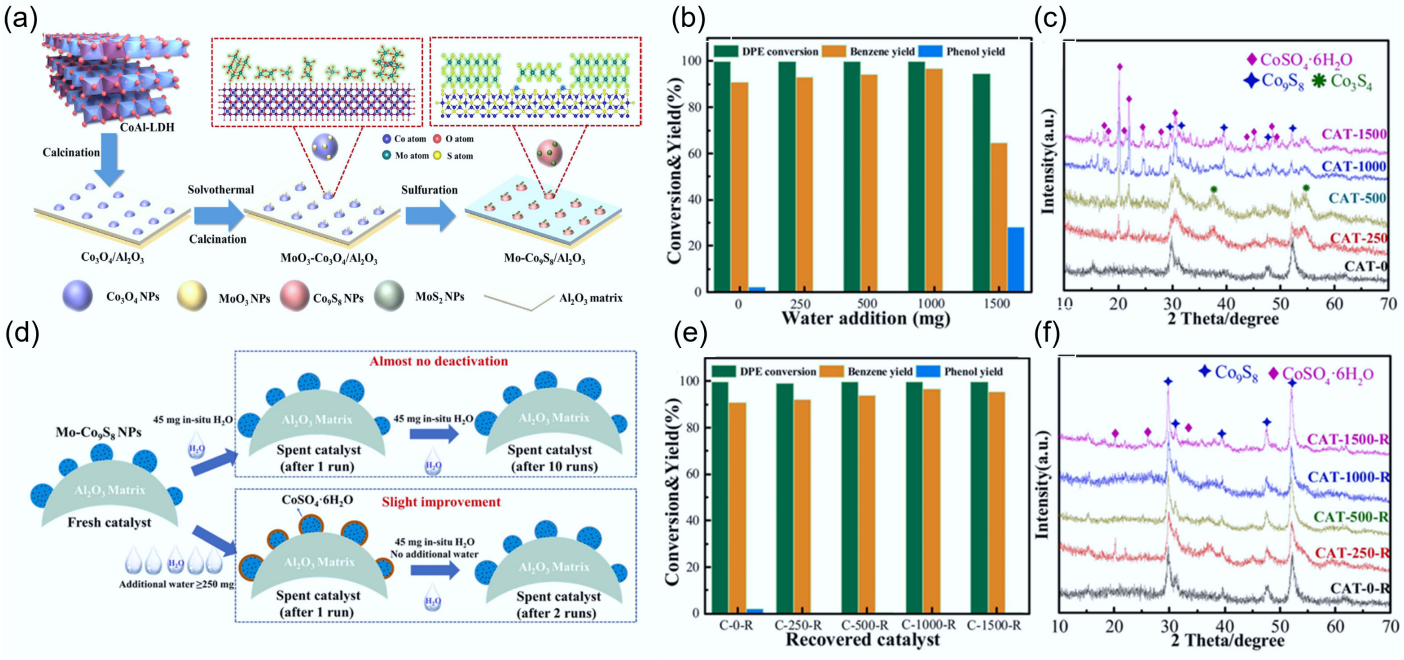

Fig. 10 (**a**) Schematic synthesis of Mo-Co_9S_8/Al_2O_3 catalyst. (**b**) Effect of water addition on the DPE HDO process over $Mo_{0.06}$-Co_9S_8/Al_2O_3 catalyst. (**c**) XRD spectrum of $Mo_{0.06}$-Co_9S_8/Al_2O_3 recovered from the (**b**) reaction. (**d**) Simplified scheme for catalyst property changes. (**e**) HDO results of $Mo_{0.06}$-Co_9S_8/Al_2O_3 catalysts recovered from the (**b**) reaction over DPE. **(f)** XRD spectrum of $Mo_{0.06}$-Co_9S_8/Al_2O_3 recovered from the (**e**) reaction. Reaction conditions: 106 mg catalyst, 3 MPa, 265 °C, 10 h. Reproduced with permission[50]. Copyright 2022, Elsevier.

In recent years, bifunctional metal-acid catalysts have garnered growing research attention and demonstrated remarkable activity in the HDO of lignin for the production of hydrocarbon compounds. It is desirable to design and synthesize bifunctional catalysts integrating the hydrogenation ability of active metals and the deoxygenation properties of Brønsted and Lewis acid sites to promote efficient HDO reactions[101–104]. Usually, the noble metals provide hydrogenation active sites for the HDO reaction, while the carriers or the incorporated second acidic oxides provide acidic sites. Zhao et al.[101] have made a significant contribution to the efficient combination of the active sites. The research team developed a bifunctional catalytic system combining carbon-supported noble metals with phosphoric acid, which achieved selective transformation of phenolic bio-oil constituents into cycloalkanes and methanol through consecutive hydrogenation–hydrolysis–dehydration pathways. The transformation of phenols to cyclohexane in liquid-phase hydrodeoxygenation occurred via a sequential three-step mechanism: (i) metal-catalyzed aromatic ring hydrogenation to cyclohexanol, (ii) acid-promoted cyclohexanol dehydration generating cycloalkene intermediates, and (iii) final metal-catalyzed hydrogenation of the cycloalkene to saturated cyclohexane[101,105].

Duan et al. prepared an efficient Pd/m-MoO_3-P_2O_5/SiO_2 catalyst for the HDO of phenol as a model substrate[52]. When compared with the Pd/SiO_2 catalyst, which only yielded hydrogenation products (cyclohexanol and cyclohexanone), the new Pd/m-MoO_3-P_2O_5/SiO_2 catalyst promoted the subsequent dehydration process. This improvement stems from the introduction of acidic sites (m-MoO_3-P_2O_5), leading to highly dispersed Pd and coexisting Brønsted–Lewis acid sites on the catalyst surface. Under mild reaction conditions, the catalyst exhibited complete phenol conversion

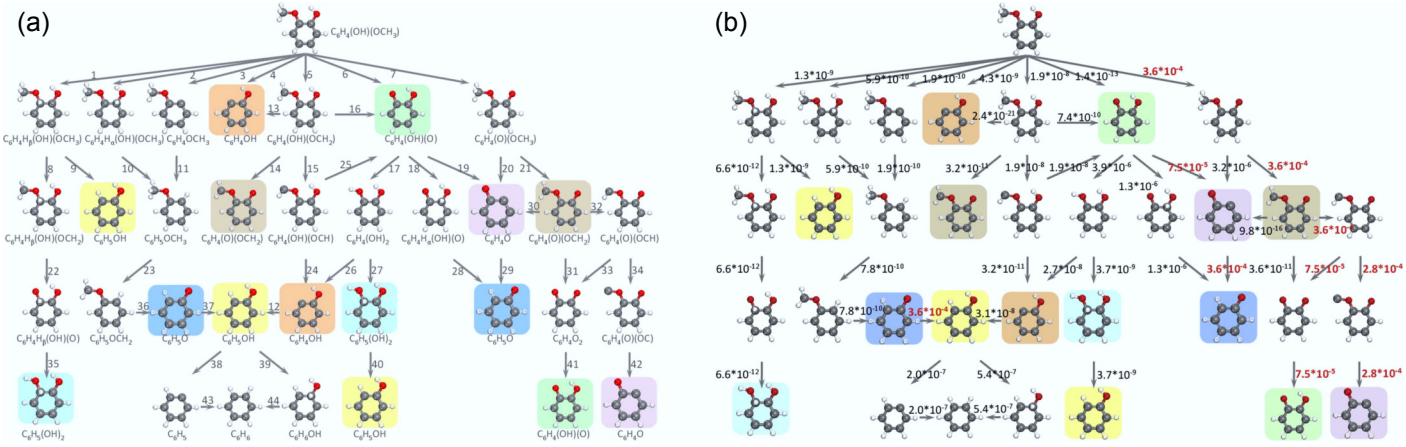

Fig. 11 **(a)** Reaction network depicting the hydrogenation of guaiacol on the Pt (111) surface to yield aromatic products. **(b)** Turnover frequencies (s^{-1}) of elementary steps at the pressure of 1 bar for guaiacol and hydrogen reactants and the temperature of 573 K. Reproduced with permission[90]. Copyright 2015, American Chemical Society.

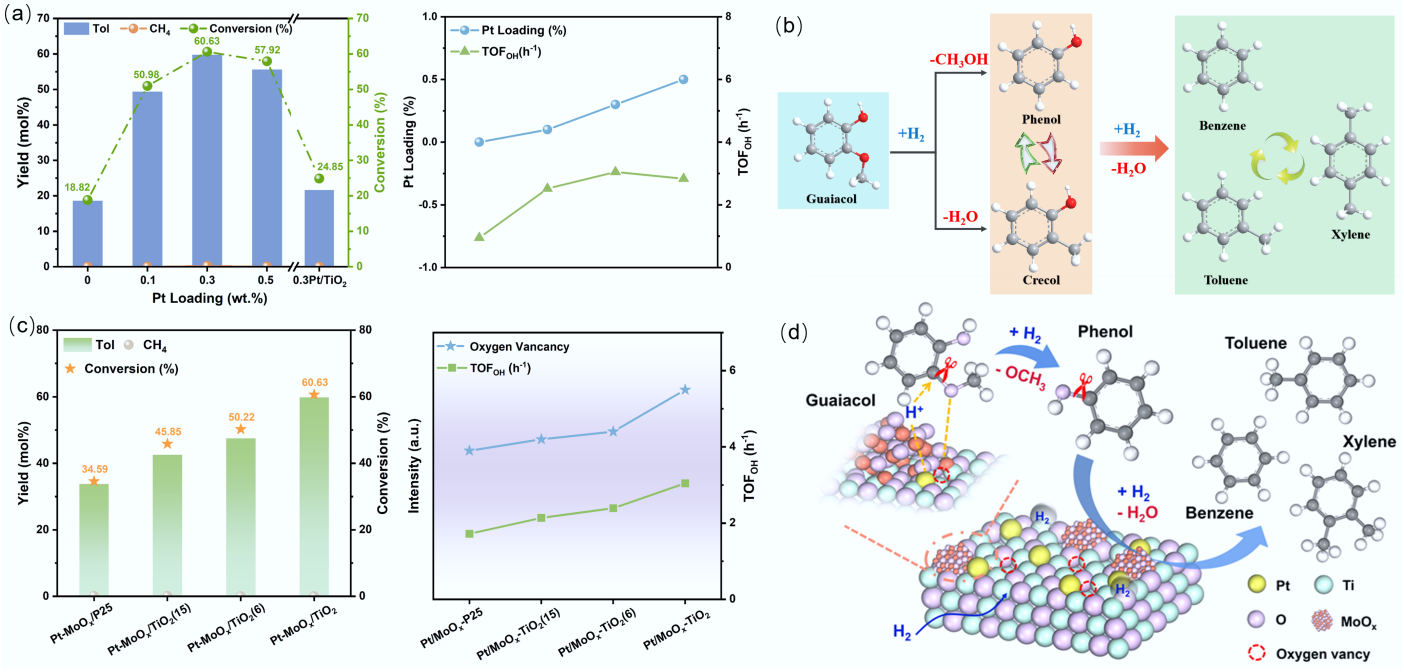

Fig. 12 (**a**) The hydrogenation dehydrogenation of guaiacol by Pt-Mo bimetallic system. (**b**) Direct deo-xygenation and alkylation transfer of guaiacol on Pt-Mo surface. (**c**) The influence of carrier oxygen vacancies on the hydrogenation dehydrogenation rate of Pt-Mo catalysts. (**d**) The synergistic mechanism of bimetallic and carrier oxygen vacancies. Reproduced with permission[100]. Copyright 2025, Wiley-VCH GmbH.

(100%) with exceptional cyclohexane selectivity (97.5%), demonstrating superior performance compared to the monofunctional Pd/SiO_2 reference system. Yang et al. strategically exploited the synergistic interplay between metallic and acidic sites by developing a bifunctional catalytic system comprising Ru/C and phosphotungstic acid (HPW)[55]. The thermally responsive phase transition characteristics of HPW facilitated its uniform distribution across the Ru/C catalyst surface while enhancing interfacial interactions between metallic and acidic active sites. Ru/C-HPW enabled the efficient conversion of guaiacol to cycloalkane products at a lower temperature (200 °C), which demonstrated the advantages of high reaction rate and good recoverability.

Molecular sieve solid acid catalysts have found wide application in bifunctional catalysts due to the unique selective morphology, strong hydrothermal stability, and tunable acidity[106,107]. The nanoscale intimacy between metallic and acidic centers in metal-molecular sieve catalysts notably enhances metal stability and enables synergistic effects in catalytic reactions. Yang et al. prepared highly dispersed (dispersion ~ 80%) ultrafine metallic Ru clusters (average particle size 1.4 nm) by an *in situ* two-stage hydrothermal synthesis strategy (Fig. 13a), and successfully encapsulated them into high-alumina ZSM-5[56]. This new method offered significant advantages over the conventional impregnation method (average particle size 11.5 nm) and the one-step hydrothermal method (average particle size 7.5 nm). It significantly improved the metal stability and prevented the sintering or leaching of active metal species during the catalytic process[108]. As shown in Fig. 13b, after thermal treatment at varying temperatures from 573 to 873 K, the average diameter of Ru species in Ru@ZSM-5 did not change significantly, even at high temperatures, and remained at 1.5 nm. This result confirms that the confined environment of molecular sieves improves the thermal stability of metal clusters. The Ru@H-ZSM-5 catalyst exhibited a narrow and distinct Al (IV) signal (99.2%), along with a Brønsted acid site (BAS) fraction of 97% in the molecular sieve pore. The Al (IV) dominated in the tetrahedral framework of aluminum (FAL), and provided tight Ru clusters and BAS neighborhoods at the sub-nanometer level. Unlike the Ru/SiO_2 catalyst without acid sites, where the phenol HDO reaction yielded only the primary products cyclohexanone and cyclohexanol, the selectivity and yield of cyclohexane in Ru@H-ZSM-5 were significantly increased (Fig. 13c), improving the ability of deep HDO.

While an increase in acidic sites can facilitate the deoxygenation process, excessively high acidity may lead to the polymerization of phenolic compounds to form coke deposits that adhere to the catalyst surface and result in coking deactivation. For example, in the HDO of guaiacol over $CoMo/Al_2O_3$ catalyst studied by Laurent & Delmon, the strong acidity of Al_2O_3 led to the polymerization of guaiacol[68]. As a typical acidic carrier, TiO_2 is moderately acidic and less prone to polymerization, and therefore has potential as a carrier of HDO catalysts[109,110]. Zhong et al. dispersed Ru on four different morphologies of TiO_2 by photochemical methods, including nanosphere (TNP), nanosheet (TNS), nanobelt (TNB), and nanocluster (TNC) (Fig. 14a-d). Ru/TNP showed good performance in the HDO of guaiacol at 250 °C and 1 MPa H_2, achieving nearly 100% conversion and cyclohexane selectivity. This exceptional activity arises from its large surface area, robust hydrogen adsorption capacity, and abundant medium-strength acid sites (Fig. 14e,f)[54].

To suppress the excessive hydrogenation of aromatic rings to generate cycloalkanes, the selectivity of aromatic hydrocarbons was significantly improved by rational modification of the catalyst structure. Bifunctional catalysts have demonstrated breakthrough progress among numerous catalytic materials in recent years due to their superior performance, becoming a research hotspot for an increasing number of scientists[111,112]. Bifunctional catalysts typically consist of two components: metals and reducible metal oxides. Among them, metals (like Pt, Pd, Ru, etc.) adsorb and activate hydrogen molecules, generating active hydrogen protons that provide additional active sites for hydrogenation reactions, and significantly enhance the reaction rate. It has been confirmed that the interaction between Pt and different metal oxides significantly affects the selectivity of target products, promoting the reaction to proceed toward the formation of specific aromatic products[113]. Reducible metal oxides markedly improve hydroxyl group adsorption capacity via engineered oxygen vacancy formation, thereby enabling

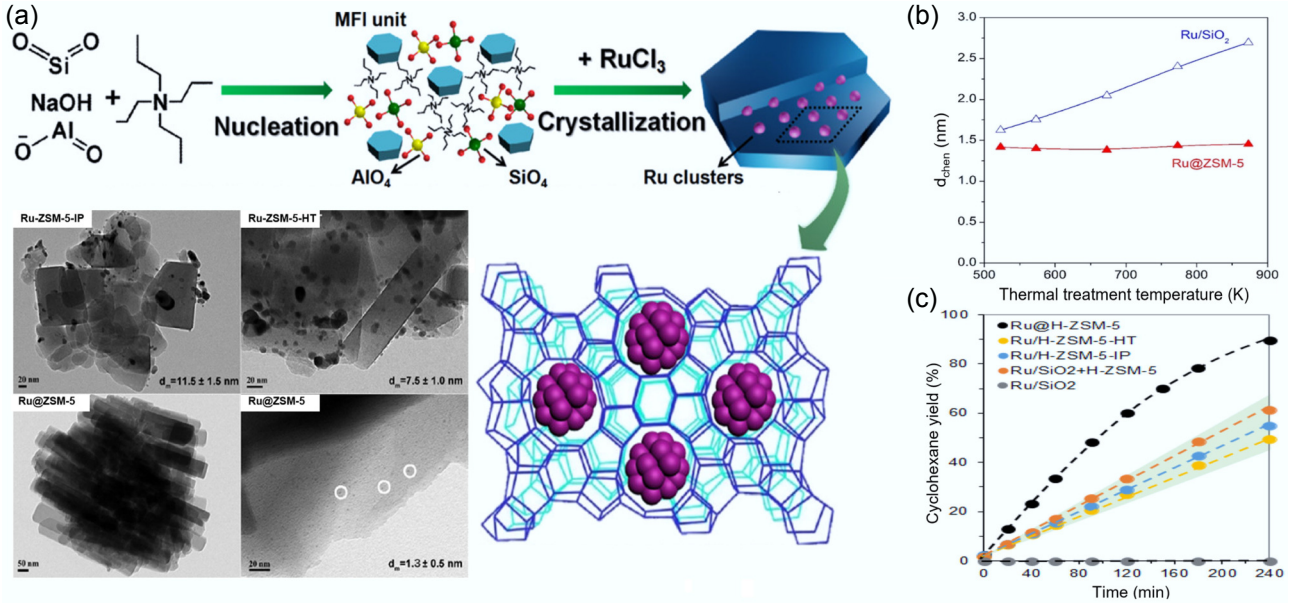

Fig. 13 (**a**) Schematic preparation and TEM characterization of catalysts for *in situ* two-stage hydrothermal synthesis of metal clusters encapsulated into high-alumina ZSM-5. (**b**) Average diameters of Ru particles in Ru/SiO_2 and Ru@ZSM-5 by H_2 chemisorption across a temperature range spanning from 573 to 873 K. (**c**) Time-dependent cyclohexane yield profiles for various catalysts. Reproduced with permission[56]. Copyright 2022, American Chemical Society.

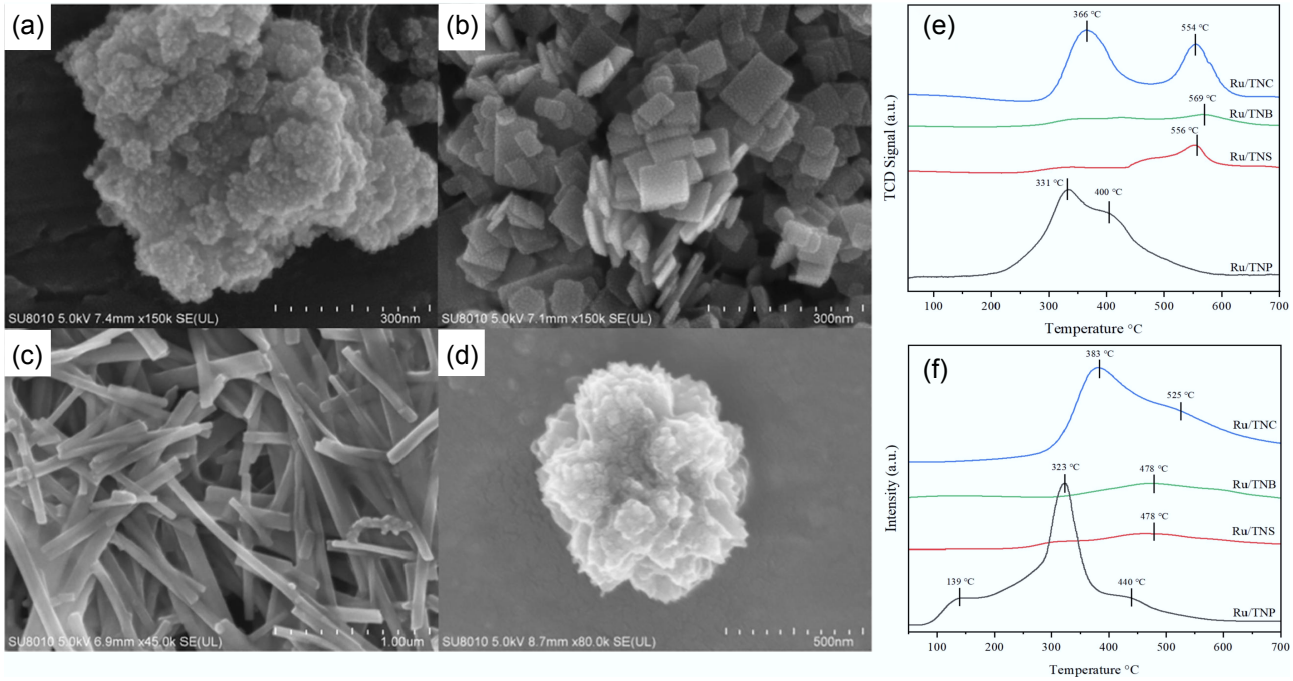

Fig. 14 SEM micrographs of: (**a**) Ru/TNP, (**b**) Ru/TNS, (**c**) Ru/TNB, (**d**) Ru/TNC. (**e**) H_2-TPD, and (**f**) NH_3-TPD patterns for different Ru-based catalysts. Reproduced with permission[54]. Copyright 2023, Elsevier.

efficient direct deoxygenation pathways under thermodynamically challenging low-pressure, high-temperature conditions[53]. At high temperatures, the C–O bond in hydroxyl groups adsorbed on oxygen vacancies gains sufficient energy to break, producing dehydroxylation products. More importantly, the close coupling between metal active sites and reducible metal oxide active sites in the bifunctional catalyst system plays a crucial role in improving the selectivity of aromatic hydrocarbons[114]. Wang et al. explored the synthesis of toluene from m-cresol via HDO reaction over C-loaded Pt-WO_x catalysts[59]. DFT calculations of m-cresol adsorption on the optimized Pt (111) surface revealed that platinum not only stabilized tungsten oxide species but also induced the generation of redox-active sites, thereby accelerating C–O bond hydrogenolysis. Thus, in stark contrast to the inferior performance of the Pt/C catalyst, which exhibited lower selectivity and stability in this reaction, the Pt-WO_x/C catalyst demonstrated remarkably high activity and toluene selectivity (> 94%). Under reduced hydrogen pressure and in the absence of a solvent, the Pt-WO_x/C catalyst still displayed exceptionally high selectivity for the target product. The authors further demonstrated that this highly active catalyst is not limited to cresol derivatives alone. In response to the problem that the aromatic rings are prone to hydrogenation during the hydrodeoxygenation of conventional lignin derivatives, Gao et al. designed a bimetallic highly targeted deoxygenation catalyst rich in oxygen vacancy defects[100]. The Pt-MoO_x/TiO_2 catalyst supported on TiO_2 rich in oxygen vacancies prepared by the hydrothermal method features a large specific surface area, pore volume, small microcrystalline size, higher acidity, and obvious mesoporous characteristics, which effectively improve the hydrodeoxygenation performance of the catalyst. The catalyst exhibits a strong signal peak intensity of oxygen vacancies, which can promote the reduction of Mo species while avoiding excessive reduction of active valence states. Under the optimal catalyst preparation and reaction conditions, the Pt-MoO_x/TiO_2 catalyst shows significantly better reaction activity than other catalysts, achieving complete conversion of m-cresol and a high aromatic hydrocarbon molar yield of 98.45%.

The introduction of heteroatoms can affect the adsorption patterns and conversion pathways of the substrates. In the HDO of diphenyl ether, Ru/C showed excellent hydrogenation performance toward the benzene ring under conditions of 120 °C, 5 bar H_2, and with methanol as a hydrogen-donor solvent[115,116]. However, the introduction of the halogenated element Br for the hydrogenolysis pretreatment of Ru/C under reducing conditions led to a dramatic change in the product distribution, with aromatic hydrocarbons (benzene and phenol) as the main products in yields as high as 90.3%, implying that Br almost completely inhibited the hydrogenation of the benzene ring[60]. FTIR spectral analysis of CO adsorption further confirmed that Br atoms were selectively deposited on the terraces of Ru nanoparticles, which effectively prevented the excessive hydrogenation of the aromatic ring (Fig. 15). The hydrogenolysis of C–O bonds primarily occurs at the corner and edge surfaces of Ru nanoparticles, where positively charged Ru species exhibit high deoxygenation activity toward these bonds.

The pore size of the catalyst also affects the aromatic selectivity. Zhang et al. demonstrated that coating well-dispersed Pd nanoparticles with porous TiO_2 films significantly improved the HDO selectivity toward the aromatic phenolic compound m-cresol (Fig. 16a, e)[117]. The porosity of TiO_2 films was modulated by adjusting the rate of water injection to regulate the hydrolysis rate of the precursor or by switching to acetone to reduce the activity of the precursor[118]. Pd@TiO_2-WI had the smallest average pore size (4.8 nm), with most (~ 82%) of them having pore widths less than 5 nm, whereas ~ 50% of Pd@TiO_2-WD with an average pore size of 8.5 nm had pore widths larger than 5 nm, and Pd@TiO_2-AI had the largest average pore size of 19.5 nm (Fig. 16b–d). They found that encapsulating Pd in TiO_2 films with a minimal pore size could suppress side reactions, accelerate the HDO reaction rate, as well as inhibit the decarboxylation and cyclic hydrogenation.

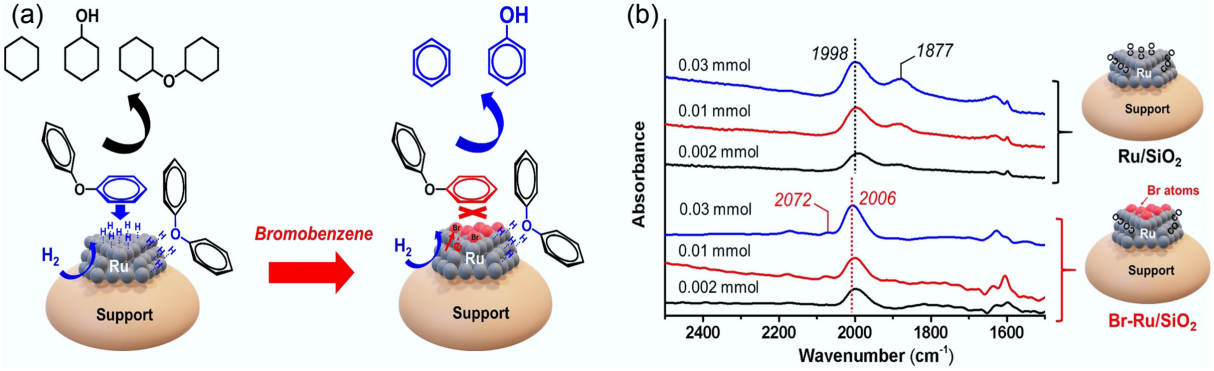

Fig. 15 (**a**) Schematic illustration of the adsorption and conversion of DPE on Ru and Ru-Br catalysts. (**b**) CO-FTIR patterns of Ru/SiO_2 and $Br\text{-}Ru/SiO_2$ catalysts. Reproduced with permission[60]. Copyright 2021, Wiley-VCH GmbH.

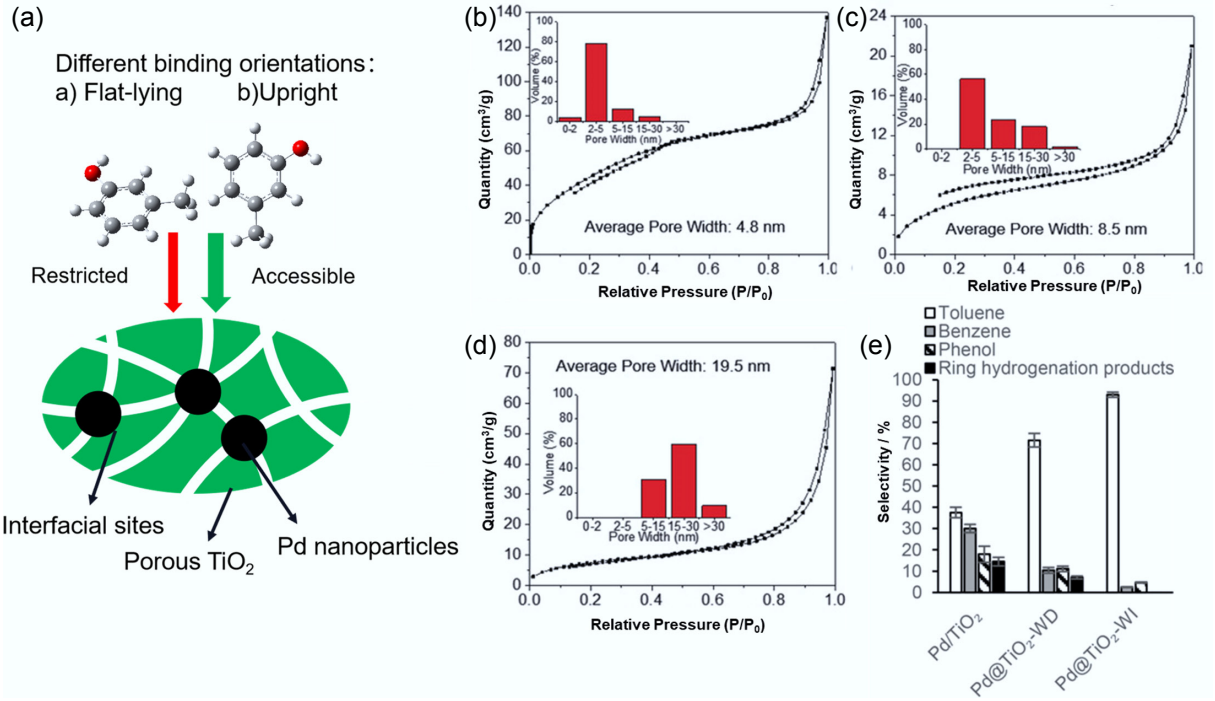

Fig. 16 (**a**) The nanoporous TiO_2 film precisely modulates binding characteristics and creates engineered interfacial active sites. N_2 physisorption isotherm plots and pore size distributions of TiO_2 in (**b**) $Pd@TiO_2$-WI, (**c**) $Pd@TiO_2$-WD, (**d**) $Pd@TiO_2$-AI. (**e**) Catalytic conversion selectivity of HDO on m-cresol. Reproduced with permission[117]. Copyright 2017, Wiley-VCH Verlag GmbH & Co. KGaA, Weinheim.

Non-noble metal catalysts

Recent studies on HDO catalysts have also centered on the development of low-cost transition metal catalysts[119,120]. Coking remains one of the most critical issues in HDO, directly impeding the industrial application of bio-oil. While elevated temperatures promote faster reaction kinetics, they concomitantly increase carbon deposition rates. Structurally optimized transition metals (Ni, Co, Mo) have shown significant effectiveness in mitigating carbon deposition during catalytic processes.

In particular, metal Ni has a strong ability to adsorb and activate H_2, and is widely used in the HDO of bio-oil model compounds. Studies have revealed that metal oxide supports notably enhance the deoxygenation activity of Ni-based catalysts. Mortensen et al. demonstrated that Ni/ZrO_2 showed the best phenol HDO performance in a range of catalysts (Ni/Al_2O_3, Ni/SiO_2, $Ni/CeO_2\text{-}ZrO_2$, Ni/CeO_2, Ni/C, Ru/C, and Pd/C). The interaction between the oxygen-friendly sites $Zr^{3+/4+}$ and the –OH bond on the ZrO_2 carrier was beneficial for the activation of phenol, thus facilitating the HDO reaction[121]. Previous studies have indicated that in a bimetallic catalyst, the active metal site facilitates H_2 dissociation, whereas the modified metal provides anchoring sites for the oxide[93, 122,123]. Chen et al.[62] designed and developed an inexpensive $FeNi\text{-}ZrO_2$ catalyst via a co-crystallization method for the production of cyclohexane from guaiacol. By adding the oxygen-friendly metal Fe, the catalytic activity for HDO was significantly improved, achieving a hydrocarbon product selectivity of 98.5% at complete guaiacol conversion. Compared with the traditional impregnation method, the co-crystallization method resulted in a stronger binding of the metal species to the amorphous zirconium dioxide and promoted metal dispersion.

The cooperative interaction between acidic and active catalytic sites was observed to facilitate selective C–O bond scission, leading to cycloalkane formation[6, 124,125]. The incorporation of phosphorus species induced both electronic modulation and geometric

restructuring of the Ni_2P phase, facilitating robust interactions between phosphorus sites and hydroxyl groups. Highly dispersed and smaller (14.7 nm) Ni_2P particles were formed, which also exposed more active sites on the catalyst surface (Fig. 17a–d). In addition, it significantly increased the acidic sites (Fig. 17e) and facilitated the dehydration of cyclohexanol to produce cyclohexane[63, 126]. The Ni_2P/SiO_2 catalyst exhibited high methylcyclohexane selectivity (96.3%) at 250 °C for 4 h. The Ni_2P (001) surface facilitates C^-OH bond cleavage with a 1.45 eV energy barrier. This result has been confirmed by DFT, demonstrating superior activity over conventional Ni (111) (2.82 eV) (Fig. 17f)[64].

Co-based catalysts also showed good activity for lignin-derived phenol hydrogenation. However, due to the weaker deoxygenation ability of Co compared to Ni, it usually requires a combination of metal doping or metal-carrier synergistic means to promote –OH breakage[128–130]. Ji et al. prepared Co-Al_2O_3@USY bifunctional catalyst via treatment of CoAl layer double hydroxide (LDH) grown *in situ* on USY molecular sieve in a reducing atmosphere (Fig. 18a)[127]. The catalytic performance was investigated in the HDO process of guaiacol under conditions of 180 °C, 3 MPa, and 4 h, achieving complete conversion with a high cyclohexane yield of 93.6%. The reduction properties of oxide precursors were further analyzed in conjunction with H_2-TPR (Fig. 18b), and it was found that a strong interaction between Co and the molecular sieve carrier was formed. Meanwhile, the topological transformation of the LDH structure produced small Co nanoparticles (average particle size of 10.6 nm) that were highly dispersed on the surface of the catalyst (Fig. 18c)[131–133]. Simultaneously, the unique properties of molecular sieves endowed the catalyst surface with abundant acidic sites (Fig. 18d), and the synergistic effect with the metal active sites improved the deoxygenation capacity. In addition, the anchoring effect of Al_2O_3 matrix on Co nanoparticles well suppressed the agglomeration of Co particles; therefore, the catalyst exhibited excellent stability. Zhang et al. also synthesized a bifunctional catalyst by combining a Ni-Co alloy with an oxygen-friendly carrier NbO_x, which showed high catalytic activity when Ni: Co = 1 (molar ratio). Notably, from the H_2-TPD profiles (Fig. 19a), it was found that the reduction peak areas of the bimetallic 5Ni-5Co/NbO_x catalyst were significantly larger than those of the monometallic ones, which was attributed to the fact that high metal loading of bimetallic catalysts leads to an increase in the consumption of H_2. The notable peak shift toward the low-temperature region indicated that the Ni-Co alloy facilitated the reduction of oxide precursors. The oxygen vacancies in NbO_x not only enhanced the adsorption of phenolics but also contributed to the formation of unique acidic sites (Fig. 19b), which promoted the HYD pathway and formed a strong interaction with the active metal to achieve the complete conversion of guaiacol, with up to 98.9% selectivity for cycloalkanes at 300 °C, 3 MPa H_2[61].

Unlike Co selectively breaks C–C bonds, one of the cheapest and abundant transition metals Fe exhibits high deoxygenation rates at low H_2 consumption and has superior selectivity toward aromatic production from phenolics[134]. Sun et al. prepared a Fe-modified

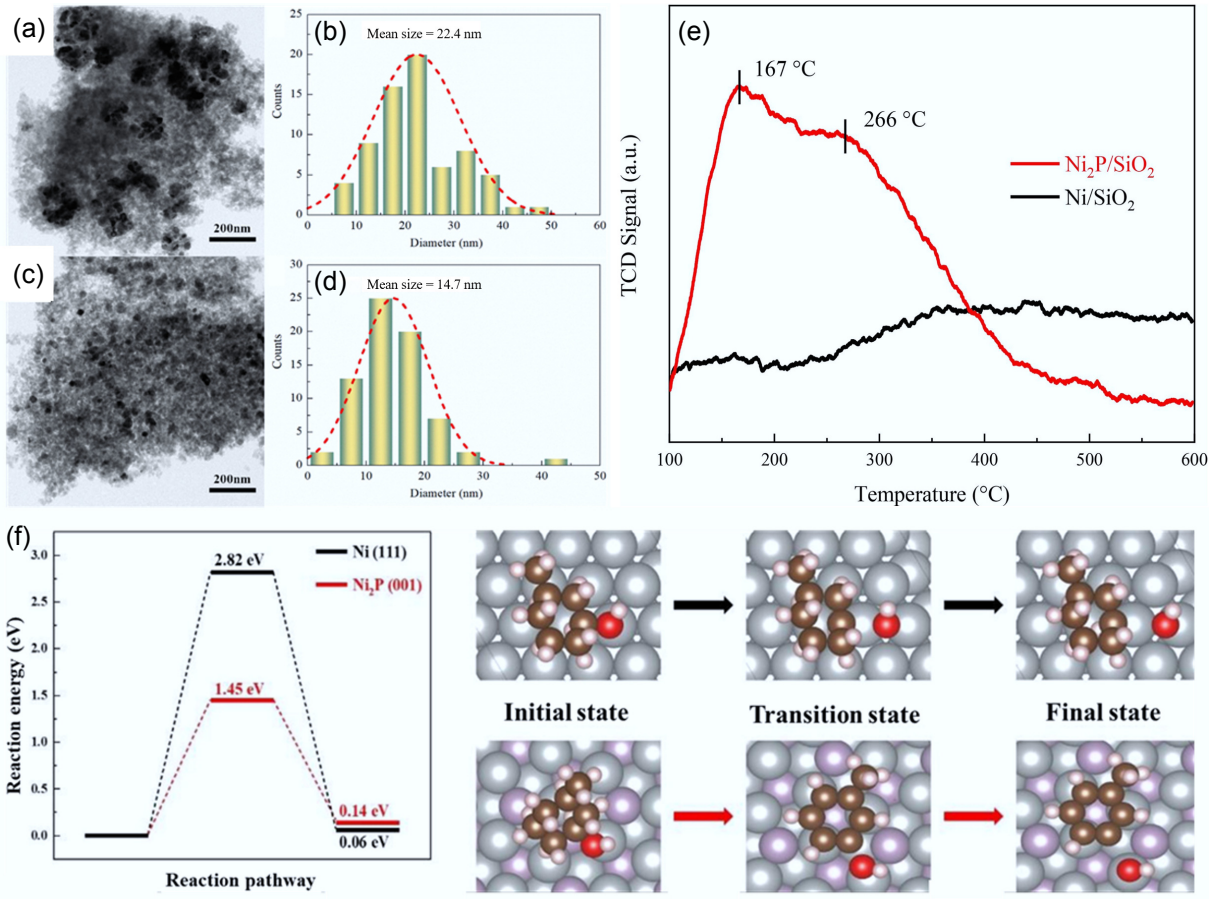

Fig. 17 (**a**) TEM images of Ni/SiO_2, and (**c**) Ni_2P/SiO_2 and respective (**b**), (**d**) particle size distributions. (**e**) NH_3-TPD profiles of Ni/SiO_2 and Ni_2P/SiO_2 catalysts. (**f**) C–OH bond cleavage energy barriers for MCHnol on the Ni (111) and Ni_2P (001) surfaces. Ni: gray, P: purple, C: brown, H: pink, O: red. Reproduced with permission[64]. Copyright 2023, Elsevier.

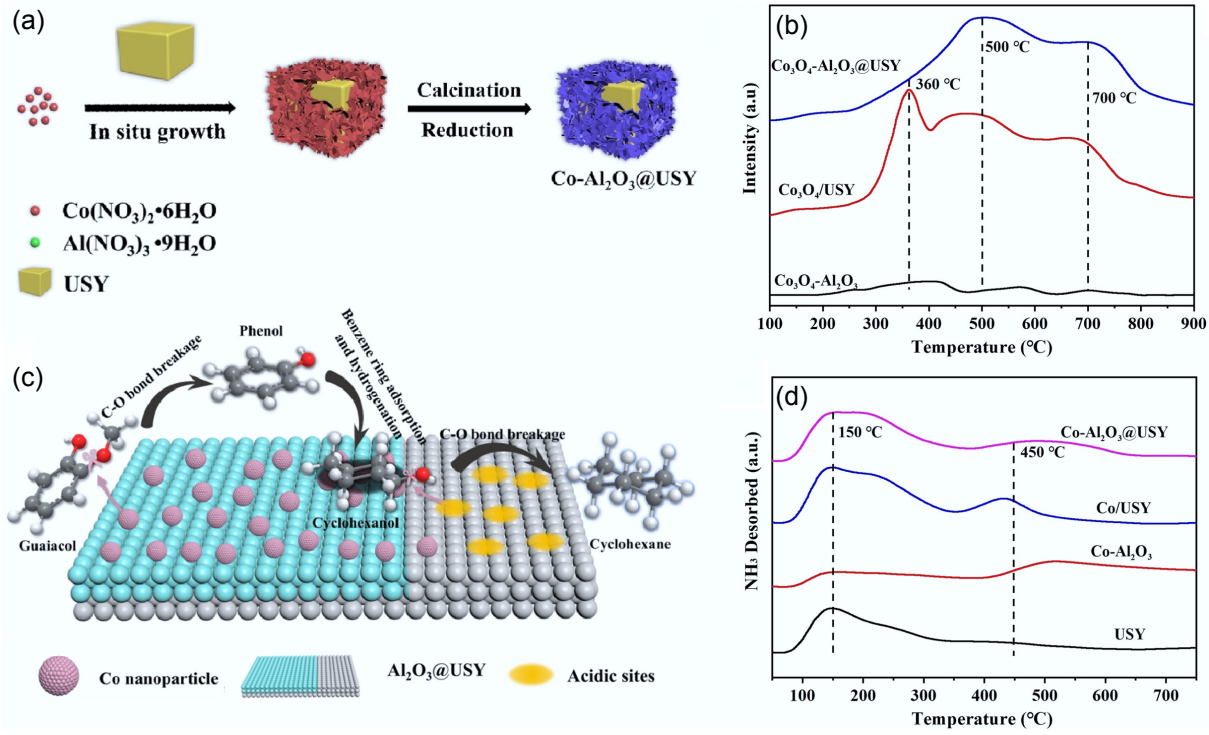

Fig. 18 (**a**) Schematic synthesis of Co-Al_2O_3@USY catalyst. (**b**) H_2-TPR profiles of Co_3O_4-Al_2O_3, Co_3O_4/USY, and Co_3O_4-Al_2O_3@USY. (**c**) Postulated reaction pathways for guaiacol hydrodeoxygenation catalyzed by the Co-Al_2O_3@USY catalyst. (**d**) NH_3-TPD profiles of USY, Co-Al_2O_3, Co/USY, and Co-Al_2O_3@USY. Reproduced with permission[127]. Copyright 2022, Wiley-VCH GmbH.

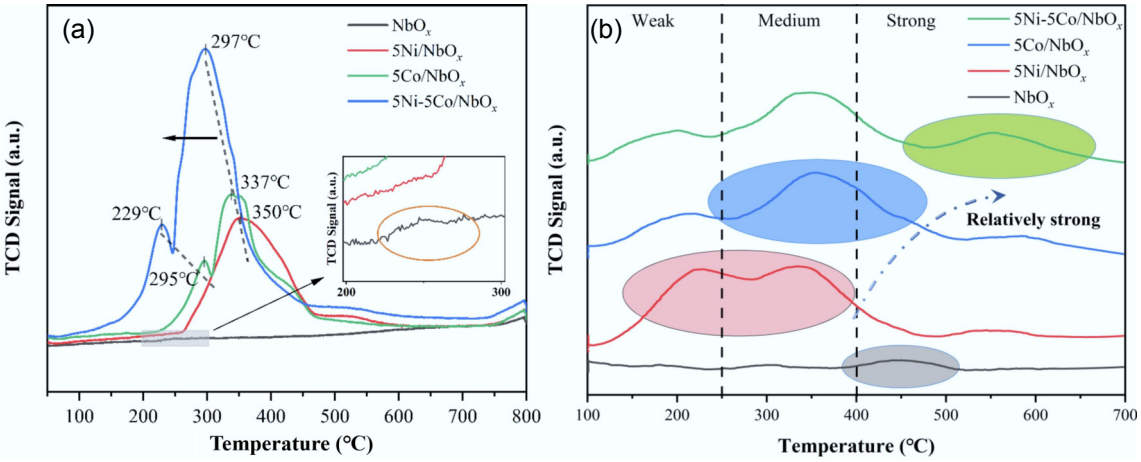

Fig. 19 (**a**) H_2-TPR, and (**b**) NH_3-TPD profiles of NbO_x, 5Ni/NbO_x, 5Co/NbO_x, and 5Ni-5Co/NbO_x catalysts. Reproduced with permission[61]. Copyright 2022, Elsevier.

ZSM-5 catalyst, which prefers C–O bond breaking as Fe is an oxygen-friendly metal, and the yield of aromatics was greatly improved[135]. The presence of Fe also led to the catalyst surface susceptible to oxidation or deactivation due to carbon deposition[110, 136–139].

Existing studies have shown that tailoring the active metal particle size significantly affects both the catalytic activity and aromatic hydrocarbon selectivity in phenolic HDO. Ni-based catalysts typically exhibit benzene ring hydrogenation at low temperatures. Unfortunately, they are prone to break C–C bonds at high temperatures to generate large amounts of the byproduct methane, resulting in a decrease in the calorific value due to the undesired carbon loss[64]. Therefore, it is important to improve HDO activity by modifying Ni-based catalysts. The correlation between Ni nanoparticle sizes (2–22 nm) supported on SiO_2 and their deoxygenation activity was systematically investigated through m-cresol hydrodeoxygenation experiments conducted at 300 °C under 1 atmosphere H_2 pressure[66]. The surface site distribution (terrace/step/corner) exhibits strong particle-size dependence, with relative abundances varying by up to 70% across the 2-22 nm range. As the Ni particle size increases, the proportion of terrace sites increases while that of corner sites decreases (Fig. 20a). A size reduction of Ni particles from 22 nm to 2 nm resulted in a 6-fold increase in toluene-selective deoxygenation TOF, concomitant with a 75% reduction in methane formation activity. Nevertheless, CH_4 selectivity remained at 10% (Fig. 20b). These findings demonstrate that

reduced particle dimensions promote deoxygenation/hydrogenation pathways, while extended terrace sites preferentially facilitate C–C bond hydrogenolysis. Reducing the Ni particle size represents an effective strategy to suppress C–C hydrogenolysis. The propensity for C–C bond hydrogenolysis can be effectively suppressed through strategic incorporation of a secondary metal to create bimetallic catalytic systems. Yang et al. designed a Ni-Mo alloy catalyst with equal molar ratio loaded on SiO_2[67]. Comparative evaluation under standardized conditions revealed that the NiMo bimetallic system achieved m-cresol conversion rates that were 10 to 20 times greater than its monometallic counterparts. Besides, it also showed high deoxygenation activity for toluene, and there was essentially no C–C hydrogenolysis reaction to CH_4 even at a high temperature of 350 °C. Overall, during HDO over a specific active metal catalyst, the metal particle size plays a decisive role in governing product distribution. Meanwhile, a higher proportion of step or corner sites on the metal surface is more conducive to the cleavage of the C–O bond.

In the hydrodeoxygenation process of guaiacol, the C_{Ar}–OCH_3 bond cleavage is kinetically favored over C_{Ar}–OH scission due to its significantly lower activation energy barrier. Since –OCH_3 of intermediate methanol and –OCH_3 of guaiacol have similar effects, they equally occupied the active sites on the catalyst surface. This strong interaction significantly weakened the adsorption of -OH groups, leading to competitive adsorption between methanol and phenol. This inhibits the further hydrogen deoxygenation (HDO) reaction of phenol to form benzene. Molybdenum trioxide (MoO_3) has been demonstrated to exhibit catalytic behavior analogous to that of molybdenum sulfide. To precisely tune catalyst acid-base properties, Tan's group engineered a MoO_x/BaO@SBA-15 system by depositing BaO onto oxygen-deficient MoO_x/SBA-15[140–142]. Oxygen-containing groups selectively bind to oxygen vacancies on the catalyst surface, where phenolics undergo selective adsorption in a 'non-planar' configuration, thereby inhibiting excessive hydrogenation of the aromatic ring (Fig. 21a). Upon full activation in H_2 for 2 h, the crystalline phase of molybdenum oxide was completely transformed from the pristine MoO_3 and transition Mo_4O_{11} phases to MoO_2 in the reduced state[143]. The synergistic combination of highly dispersed MoO_x species and the high-surface-area, large-pore SBA-15 support substantially increased the population of accessible

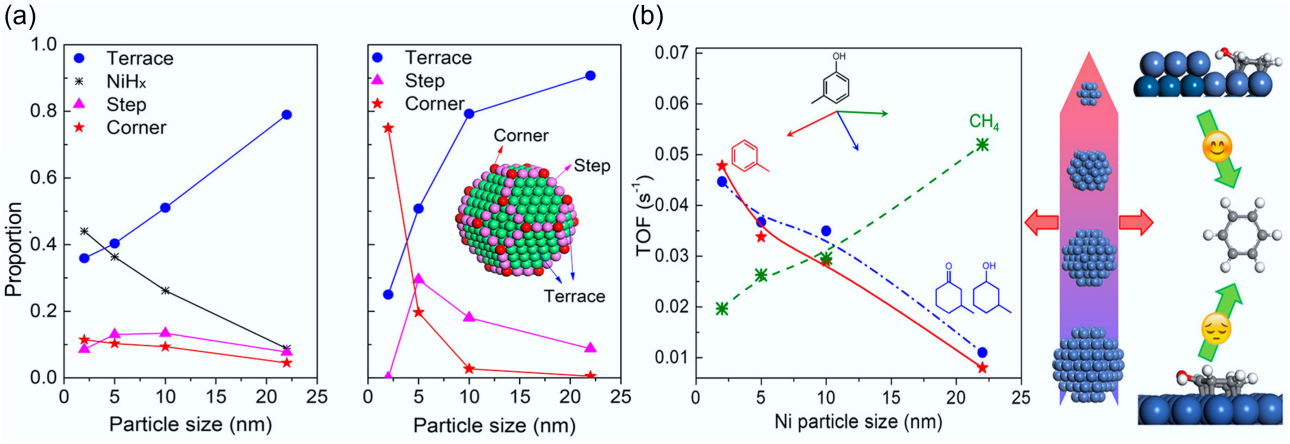

Fig. 20 (**a**) Turnover frequency (s^{-1}) for conversion of m-cresol to different products. Reaction conditions: 573 K, 0.1 MPa H_2, 30 min, W/F was adjusted to achieve conversion < 10%. (**b**) Percentage of different surface sites based on H_2-TPD patterns and theoretical percentage of the cube-octahedron model based on the size of Ni. Reproduced with permission[66]. Copyright 2018, American Chemical Society.

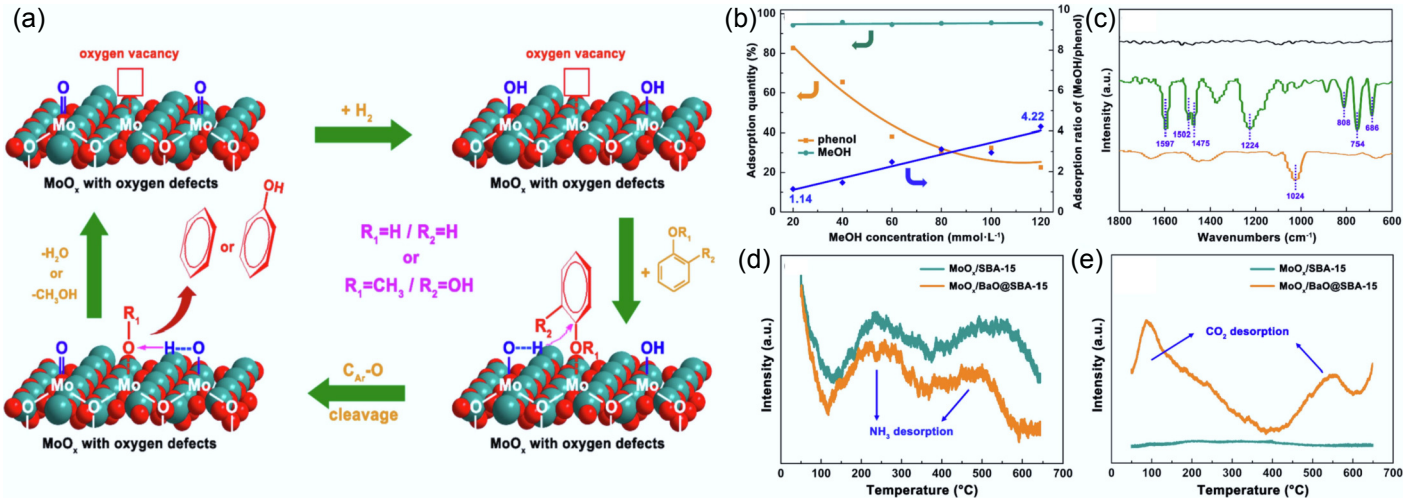

Fig. 21 (**a**) Postulated reaction mechanisms for phenolic compound hydrodeoxygenation catalyzed by activated MoO_x/SBA-15 and MoO_x/BaO@SBA-15. (**b**) Adsorption of phenol and methanol on activated MoO_x/SBA-15 under varying methanol concentrations. (**c**) FT-IR spectra of activated MoO_3 (black), activated MoO_3 treated with phenol dissolved in 1,2,4-trimethylbenzene (green), and activated MoO_3 treated with phenol dissolved in methanol (yellow). (**d**) NH_3-TPD, and (**e**) CO_2-TPD of MoO_x/SBA-15 and MoO_x/BaO@SBA-15. Reproduced with permission[140]. Copyright 2022, Elsevier.

active sites in the catalytic system. The competitive adsorption behavior between methanol and phenol was explored in solutions with different methanol concentrations, and the adsorption of methanol was consistently stabilized at 95% and above (Fig. 21b), which confirmed that the catalyst was more preferentially adsorbed over phenol for methanol. Simultaneously, FT-IR spectra also yielded consistent findings (Fig. 21c). In the samples treated with both phenol and methanol, the characteristic signal peaks of adsorbed phenol completely disappeared. The catalyst had a stronger interaction with methanol and then inhibited the HDO reaction. The BaO coating enhanced the alkalinity of the catalyst surface (Fig. 21d,e), which promoted the adsorption of phenol. The intermediate product methanol can be eliminated by alkylation reaction with phenol, which further enhances the one-step generation of aromatic products from guaiacol.

Among the numerous factors leading to catalyst deactivation, sintering of active components is considered as one of the most dominant causes[144]. Recent advances in catalyst design have increasingly targeted core-shell architectures to simultaneously address sintering resistance and active phase stabilization, while providing exceptional coking mitigation capabilities[145,146]. The core retains acidic sites to drive aromatization reactions, while the mesoporous shell layer optimizes the mass transfer pathways and improves the diffusion efficiency of reaction substrates[147,148]. Owing to its unique chemical inertness, mesoporous silica is recognized as an optimal inorganic material for encapsulating active components. This feature ensures that core components exhibit their intrinsic catalytic performance, while the shell layer effectively suppresses sintering and loss of active components[149,150]. Owing to the unique spatial constraints imposed by the core-shell architecture, lignin pyrolysis gas first contacts the shell layer upon passing through the catalyst. The large pore size of the shell layer then cleaves macromolecular oxygenates into small-molecule intermediates. These intermediates then diffuse to the internal core region for deep targeted deoxygenation[151]. Wang's research group engineered a high-performance core-shell Ni@Al_x-mSiO_2 bifunctional catalyst through precise encapsulation of Ni nanoparticles within aluminum-incorporated mesostructured silica[152]. The appropriate mesoporous pore size significantly promotes the transport of substrates and products while exposing more acidic sites to enhance their accessibility. The core-shell structure strengthens the metal-support interaction, effectively inhibiting the agglomeration of Ni nanoparticles and promoting the generation of more active sites. These characteristics endow the catalyst with excellent stability and good reusability[153,154]. Through templated synthesis, Xue and colleagues fabricated a dual-metal-loaded core-shell catalytic system specifically designed for efficient enzymatic lignin pyrolysis[155]. The research revealed that the metal type and loading position in the core-shell structure significantly influence product distribution. Loading iron on the microporous core and magnesium on the mesoporous shell provides acidic and basic sites, respectively, forming a unique acid-base synergistic catalytic system. The design of the FeZ@MgM core-shell catalyst significantly improves deoxygenation efficiency, achieving a selectivity of 38.9% for monocyclic aromatic hydrocarbons (MAHs).

Conclusions and perspectives

Hydrodeoxygenation can convert complex, unstable lignin derivatives into platform chemicals or fuels. The hydrodeoxygenation process faces multiple challenges, including demanding operational parameters (elevated temperatures and pressures), substantial hydrogen requirements, solvent usage and separation, excessive hydrogenation, and catalyst deactivation. To solve these key problems, researchers have developed a series of catalysts and uncovered the hydrogenation-deoxygenation (HDO) reaction mechanisms operative at distinct catalytically active sites. This comprehensive review systematically examines recent advancements in the heterogeneous catalytic hydrodeoxygenation of lignin-derived compounds, encompassing sulfide-based, noble metal (e.g., Pt, Pd, Ru, etc.), and non-noble metal (e.g., Ni, Co, Mo, etc.) catalyst systems. For metal sulfides, continuous addition of H_2S/C_2S is required due to the loss of S species during the reaction process. Furthermore, the catalysts are prone to deactivation due to carbon deposition (coking) or contamination. While noble metal catalysts exhibit efficient low-temperature deoxygenation activity, their propensity for particle agglomeration and rapid deactivation necessitates the incorporation of secondary metals for stabilization. The substantial economic costs and finite natural abundance of noble metals fundamentally limit their viability for industrial-scale deployment and commercial applications. Non-noble metal catalysts generally display inferior activity for the hydrodeoxygenation of lignin-derived phenolic compounds, their active phases being susceptible to oxidative degradation under low temperatures. In contrast to noble metals, these catalysts are prone to compromised stability, while promoting undesirable side reactions, including condensation and arene ring scission. Bimetallic and metal-acid bifunctional catalysts are currently the most studied catalysts for HDO reactions. Incorporating a second metal with distinct hydrotreating or oxygenophilic properties to fabricate bimetallic or intermetallic catalysts can modify the active sites of the primary metal while simultaneously generating extra active sites. The following aspects should be further explored in the future:

(1) The development of more economical, recyclable, and highly stable catalysts is essential for scaling up lignin hydrodeoxygenation processes. Enhancing HDO efficiency under mild conditions can significantly reduce energy consumption, thereby improving process economics. While noble metals can significantly increase HDO activity at low temperatures with superior resistance to deactivation, they are expensive. Consequently, a key challenge lies in improving noble metal utilization efficiency or developing cost-effective catalysts with noble metal-like performance. Phosphide catalysts have shown similar catalytic properties to noble metals and are promising for broad application in HDO reactions in the future. Acidic sites can promote the deoxygenation process, but highly acidic catalysts also accelerate the rate of coke production. Suitable mesoporous carriers also have a significant impact on catalytic performance. Large pore sizes lead to coking and deactivation, while smaller pore sizes reduce the reaction rate. Therefore, it is necessary to precisely regulate the multiple active sites of the lignin HDO catalyst to construct a highly active and stable catalyst.

(2) Exploring a more environmentally friendly strategy for hydrogen production or choosing the right solvent for the hydrogen donor would greatly improve the carbon mitigation benefits of hydrodeoxygenation (HDO) processes. Currently, the majority of industrial hydrogen is produced from fossil feedstocks, resulting in significant carbon emissions during hydrodeoxygenation (HDO) processes. Thus, there is a need to explore a more environmentally benign and viable strategy for hydrogen production or to select a suitable hydrogen donor, such as isopropanol, methanol, and other alcoholic solvents. In addition, most of the HDO reactions need to be carried out under high H_2 pressure conditions. The pursuit of atmospheric-pressure reaction conditions warrant thorough investigation, as successful implementation would simultaneously achieve significant cost reduction and enhanced operational safety.

(3) The choice of lignocellulosic biomass or lignin as a reactant is essential. Currently, a number of experiments were performed using of lignin-derived model compounds. However, real lignin and biomass compositions are very complex, leading to issues such as inadequate contact between the raw materials and the catalyst, as well as a tendency for intermediate products to undergo secondary polymerization. An efficient catalyst should be designed and developed for simultaneous application in both lignin depolymerization and subsequent hydrodeoxygenation processes to achieve the conversion of biomass to hydrocarbon target products through one-step catalysis.

(4) Actual industrial production and large-scale applications require the use of continuous reactor systems. Currently, hydrogen deoxygenation reactions at the laboratory scale are achieved through small high-pressure reactors or easily operated batch reactors. However, in large-scale bio-oil production processes, it is necessary to design reactors for continuous operation, which will facilitate higher yields of the target product. Clearly, this is challenging and requires addressing issues of heat transfer and mass transfer as well as integration with other processes.

Author contributions

The authors confirm their contributions to the paper as follows: study design: Gao Y, Xiao R, Yu J; draft manuscript preparation: Gao Y, Xiao R; data collection: Zhang H; manuscript revision: Zhang H, Yu J. All authors reviewed the results and approved the final version of the manuscript

Data availability

All data needed to evaluate the conclusions in the paper are present in the paper. Additional data related to this paper are available from the authors on reasonable request.

Funding

The authors acknowledge the financial support of National Key Research and Development Program of China (2024YFB4206205), the National Natural Science Fund for Distinguished Young Scholars of China (52425607), and the Natural Science Foundation of Jiangsu Province (BK20240010).

Declarations

Competing interests

The authors declare that there is no conflict of interest.

Author details

Key Laboratory of Energy Thermal Conversion and Control of Ministry of Education, School of Energy and Environment, Southeast University, Nanjing 210096, China

References

[1] Han X, Guo Y, Liu X, Xia Q, Wang Y. 2019. Catalytic conversion of lignocellulosic biomass into hydrocarbons: a mini review. *Catalysis Today* 319:2–13

[2] Wei J, Wang M, Wang F, Song X, Yu G, et al. 2021. A review on reactivity characteristics and synergy behavior of biomass and coal Co-gasification. *International Journal of Hydrogen Energy* 46:17116–17132

[3] Tezer Ö, Karabağ N, Öngen A, Çolpan CÖ, Ayol A. 2022. Biomass gasification for sustainable energy production: a review. *International Journal of Hydrogen Energy* 47:15419–15433

[4] Kim JY, Lee HW, Lee SM, Jae J, Park YK. 2019. Overview of the recent advances in lignocellulose liquefaction for producing biofuels, bio-based materials and chemicals. *Bioresource Technology* 279:373–384

[5] Wang M, Wang F. 2019. Catalytic scissoring of lignin into aryl monomers. *Advanced Materials* 31:e1901866

[6] Yue X, Zhang L, Sun L, Gao S, Gao W, et al. 2021. Highly efficient hydrodeoxygenation of lignin-derivatives over Ni-based catalyst. *Applied Catalysis B: Environmental* 293:120243

[7] He Z, Li Y, Liu C, Li Y, Qian M, et al. 2021. Controllable conversion of biomass to lignin-silica hybrid nanoparticles: High-performance renewable dual-phase fillers. *Waste Management* 135:381–388

[8] Li F, Zhao Y, Xue L, Ma F, Dai SY, et al. 2022. Microbial lignin valorization through depolymerization to aromatics conversion. *Trends Biotechnol* 40:1469–1487

[9] Qiu B, Tao X, Wang J, Liu Y, Li S, et al. 2022. Research progress in the preparation of high-quality liquid fuels and chemicals by catalytic pyrolysis of biomass: A review. *Energy Conversion and Management* 261:115647

[10] Provin AP, dos Reis VO, Hilesheim SE, Bianchet RT, de Aguiar Dutra AR, et al. 2021. Use of bacterial cellulose in the textile industry and the wettability challenge-a review. *Cellulose* 28:8255–8274

[11] Carpenter AW, de Lannoy CF, Wiesner MR. 2015. Cellulose nanomaterials in water treatment technologies. *Environmental Science & Technology* 49:5277–5287

[12] Wan Azelee NI, Mahdi HI, Cheng Y-S, Nordin N, Illias RM, et al. 2023. Biomass degradation: Challenges and strategies in extraction and fractionation of hemicellulose. *Fuel* 339:126982

[13] Rao J, Lv Z, Chen G, Peng F. 2023. Hemicellulose: Structure, chemical modification, and application. *Progress in Polymer Science* 140:101675

[14] Chin M, Suh SM, Fang Z, Hegg EL, Diao T. 2022. Depolymerization of lignin via a microscopic reverse biosynthesis pathway. *ACS Catalysis* 12:2532–2539

[15] Ullah M, Liu P, Xie S, Sun S. 2022. Recent advancements and challenges in lignin valorization: Green routes towards sustainable bioproducts. *Molecules* 27:6055

[16] Phan DP, Lee EY. 2020. Controlled hydrogenolysis over heterogeneous catalysts for lignin valorization. *Catalysis Reviews* 62:607–630

[17] Zong P, Jiang Y, Tian Y, Li J, Yuan M, et al. 2020. Pyrolysis behavior and product distributions of biomass six group components: Starch, cellulose, hemicellulose, lignin, protein and oil. *Energy Conversion and Management* 216:112777

[18] Gao Z, Zhou Z, Wang M, Shang N, Gao W, et al. 2023. Highly dispersed Pd anchored on heteropolyacid modified ZrO2 for high efficient hydrodeoxygenation of lignin-derivatives. *Fuel* 334:126768

[19] Marsman JH, Wildschut J, Mahfud F, Heeres HJ. 2007. Identification of components in fast pyrolysis oil and upgraded products by comprehensive two-dimensional gas chromatography and flame ionisation detection. *Journal of Chromatography A* 1150:21–27

[20] Zhang Q, Chang J, Wang T, Xu Y. 2007. Review of biomass pyrolysis oil properties and upgrading research. *Energy Conversion and Management* 48:87–92

[21] de Wild P, Van der Laan R, Kloekhorst A, Heeres E. 2009. Lignin valorisation for chemicals and (transportation) fuels via (catalytic) pyrolysis and hydrodeoxygenation. *Environmental Progress & Sustainable Energy* 28:461–469

[22] Mortensen PM, Grunwaldt JD, Jensen PA, Knudsen KG, Jensen AD. 2011. A review of catalytic upgrading of bio-oil to engine fuels. *Applied Catalysis A: General* 407:1–19

[23] Moud PH, Kantarelis E, Andersson KJ, Engvall K. 2018. Biomass pyrolysis gas conditioning over an iron-based catalyst for mild deoxygenation and hydrogen production. *Fuel* 211:149–158

[24] Valle B, Remiro A, García-Gómez N, Gayubo AG, Bilbao J. 2019. Recent research progress on bio-oil conversion into bio-fuels and raw chemicals: a review. *Journal of Chemical Technology and Biotechnology* 94:670–689

[25] Yildiz G, Pronk M, Djokic M, van Geem KM, Ronsse F, et al. 2013. Validation of a new set-up for continuous catalytic fast pyrolysis of biomass coupled with vapour phase upgrading. *Journal of Analytical and Applied Pyrolysis* 103:343–351

[26] Prajitno H, Insyani R, Park J, Ryu C, Kim J. 2016. Non-catalytic upgrading of fast pyrolysis bio-oil in supercritical ethanol and combustion behavior of the upgraded oil. *Applied Energy* 172:12–22

[27] Zhu X, Lobban LL, Mallinson RG, Resasco DE. 2011. Bifunctional transalkylation and hydrodeoxygenation of anisole over a Pt/HBeta catalyst. *Journal of Catalysis* 281:21–29

[28] Chen L, Wang C, Shang N, Gao S, Wang C. 2025. Highly dispersed Cu supported on urchin-like TiO2 for efficient hydrodeoxygenation of lignin derivatives. *Journal of Catalysis* 448:116216

[29] Rahimi A, Ulbrich A, Coon JJ, Stahl SS. 2014. Formic-acid-induced depolymerization of oxidized lignin to aromatics. *Nature* 515:249–252

[30] Ambursa MM, Sudarsanam P, Voon LH, Hamid SBA, Bhargava SK. 2017. Bimetallic Cu-Ni catalysts supported on MCM-41 and Ti-MCM-41 porous materials for hydrodeoxygenation of lignin model compound into transportation fuels. *Fuel Processing Technology* 162:87–97

[31] Zhang J, Sun J, Wang Y. 2020. Recent advances in the selective catalytic hydrodeoxygenation of lignin-derived oxygenates to arenes. *Green Chemistry* 22:1072–1098

[32] Furimsky E. 2000. Catalytic hydrodeoxygenation. *Applied Catalysis A: General* 199:147–190

[33] Zhang J, Sun J, Sudduth B, Pereira Hernandez X, Wang Y. 2020. Liquid-phase hydrodeoxygenation of lignin-derived phenolics on Pd/Fe: a mechanistic study. *Catalysis Today* 339:305–311

[34] Sun Z, Fridrich B, de Santi A, Elangovan S, Barta K. 2018. Bright side of lignin depolymerization: Toward new platform chemicals. *Chemical Reviews* 118:614–678

[35] Massoth FE, Politzer P, Concha MC, Murray JS, Jakowski J, et al. 2006. Catalytic hydrodeoxygenation of methyl-substituted phenols: correlations of kinetic parameters with molecular properties. *Journal of Physical Chemistry B* 110:14283–14291

[36] Nelson RC, Baek B, Ruiz P, Goundie B, Brooks A, et al. 2015. Experimental and theoretical insights into the hydrogen-efficient direct hydrodeoxygenation mechanism of phenol over Ru/TiO_2. *ACS Catalysis* 5:6509–6523

[37] Saidi M, Samimi F, Karimipourfard D, Nimmanwudipong T, Gates BC, et al. 2014. Upgrading of lignin-derived bio-oils by catalytic hydrodeoxygenation. *Energy & Environmental Science* 7:103–129

[38] Liu W, You W, Sun W, Yang W, Korde A, et al. 2020. Ambient-pressure and low-temperature upgrading of lignin bio-oil to hydrocarbons using a hydrogen buffer catalytic system. *Nature Energy* 5:759–767

[39] Wang H, Zhao W, Rehman MU, Liu W, Xu Y, et al. 2022. Copper phyllosilicate nanotube catalysts for the chemosynthesis of cyclohexane via hydrodeoxygenation of phenol. *ACS Catalysis* 12:4724–4736

[40] Luo Z, Zheng Z, Wang Y, Sun G, Jiang H, et al. 2016. Hydrothermally stable Ru/HZSM-5-catalyzed selective hydrogenolysis of lignin-derived substituted phenols to bio-arenes in water. *Green Chemistry* 18:5845–5858

[41] Zheng Z, Luo Z, Zhao C. 2018. Morphologically cross-shaped Ru/HZSM-5 catalyzes tandem hydrogenolysis of guaiacol to benzene in water. *ChemCatChem* 10:1376–1384

[42] Bui VN, Toussaint G, Laurenti D, Mirodatos C, Geantet C. 2009. Co-processing of pyrolisis bio oils and gas oil for new generation of biofuels: hydrodeoxygenation of guaïacol and SRGO mixed feed. *Catalysis Today* 143:172–178

[43] Runnebaum RC, Nimmanwudipong T, Block DE, Gates BC. 2012. Catalytic conversion of compounds representative of lignin-derived bio-oils: a reaction network for guaiacol, anisole, 4-methylanisole, and cyclohexanone conversion catalysed by Pt/γ-Al_2O_3. *Catalysis Science & Technology* 2:113–118

[44] Elliott DC. 2007. Historical developments in hydroprocessing bio-oils. *Energy & Fuels* 21:1792–1815

[45] Choudhary TV, Phillips CB. 2011. Renewable fuels via catalytic hydrodeoxygenation. *Applied Catalysis A: General* 397:1–12

[46] Hicks JC. 2011. Advances in C–O bond transformations in lignin-derived compounds for biofuels production. *The Journal of Physical Chemistry Letters* 2:2280–2287

[47] Venkatakrishnan VK, Delgass WN, Ribeiro FH, Agrawal R. 2015. Oxygen removal from intact biomass to produce liquid fuel range hydrocarbons via fast-hydropyrolysis and vapor-phase catalytic hydrodeoxygenation. *Green Chemistry* 17:178–183

[48] Liu G, Robertson AW, Li MMJ, Kuo WCH, Darby MT, et al. 2017. MoS_2 monolayer catalyst doped with isolated Co atoms for the hydrodeoxygenation reaction. *Nature Chemistry* 9:810–816

[49] Cao J, Zhang Y, Liu X, Zhang C, Li Z. 2023. Comparison of Co-Mo-S and remote control model for designing efficient Co-doped MoS_2 hydrodeoxygenation catalysts. *Fuel* 334:126640

[50] Diao X, Ji N, Li X, Rong Y, Zhao Y, et al. 2022. Fabricating high temperature stable Mo-Co_9S_8/Al_2O_3 catalyst for selective hydrodeoxygenation of lignin to arenes. *Applied Catalysis B: Environmental* 305:121067

[51] Wu K, Li X, Wang W, Huang Y, Jiang Q, et al. 2022. Creating edge sites within the basal plane of a MoS_2 catalyst for substantially enhanced hydrodeoxygenation activity. *ACS Catalysis* 12:8–17

[52] Duan H, Dong J, Gu X, Peng YK, Chen W, et al. 2017. Hydrodeoxygenation of water-insoluble bio-oil to alkanes using a highly dispersed Pd-Mo catalyst. *Nature Communications* 8:591

[53] Sun M, Zhang Y, Liu W, Zhao X, Luo H, et al. 2022. Synergy of metallic Pt and oxygen vacancy sites in Pt–WO_{3-x} catalysts for efficiently promoting vanillin hydrodeoxygenation to methylcyclohexane. *Green Chemistry* 24:9489–9495

[54] Zhong Z, Li J, Jian M, Shu R, Tian Z, et al. 2023. Hydrodeoxygenation of lignin-derived phenolic compounds over Ru/TiO_2 catalyst: Effect of TiO_2 morphology. *Fuel* 333:126241

[55] Yang Z, Luo B, Shu R, Zhong Z, Tian Z, et al. 2022. Synergistic effect of active metal–acid sites on hydrodeoxygenation of lignin-derived phenolic compounds under mild conditions using Ru/C-HPW catalyst. *Fuel* 319:123617

[56] Yang J, He Y, He J, Liu Y, Geng H, et al. 2022. Enhanced catalytic performance through in situ encapsulation of ultrafine Ru clusters within a high-aluminum zeolite. *ACS Catalysis* 12:1847–1856

[57] Teles CA, de Souza PM, Rabelo-Neto RC, Teran A, Jacobs G, et al. 2021. Hydrodeoxygenation of lignin-derived compound mixtures on Pd-supported on various oxides. *ACS Sustainable Chemistry & Engineering* 9:12870–12884

[58] de Souza PM, Rabelo-Neto RC, Borges LEP, Jacobs G, Davis BH, et al. 2015. Role of keto intermediates in the hydrodeoxygenation of phenol over Pd on oxophilic supports. *ACS Catalysis* 5:1318–1329

[59] Wang C, Mironenko AV, Raizada A, Chen T, Mao X, et al. 2018. Mechanistic study of the direct hydrodeoxygenation of m-cresol over WOx-decorated Pt/C catalysts. *ACS Catalysis* 8:7749–7759

[60] Wu D, Wang Q, Safonova OV, Peron DV, Zhou W, et al. 2021. Lignin compounds to monoaromatics: Selective cleavage of C-O bonds over a brominated ruthenium catalyst. *Angewandte Chemie-International Edition* 60:12513–12523

[61] Zhang C, Zhang X, Wu J, Zhu L, Wang S. 2022. Hydrodeoxygenation of lignin-derived phenolics to cycloalkanes over Ni–Co alloy coupled with oxophilic NbO_x. *Applied Energy* 328:120199

[62] Chen Q, Cai C, Zhang X, Zhang Q, Chen L, et al. 2020. Amorphous FeNi-ZrO_2-catalyzed hydrodeoxygenation of lignin-derived phenolic compounds to naphthenic fuel. *ACS Sustainable Chemistry & Engineering* 8:9335–9345

[63] Gonçalves VOO, de Souza PM, Cabioc'h T, da Silva VT, Noronha FB, et al. 2017. Hydrodeoxygenation of m-cresol over nickel and nickel phosphide based catalysts. Influence of the nature of the active phase and the support. *Applied Catalysis B: Environmental* 219:619–628

[64] Zhu T, Liu K, Wang H, Wang J, Li F, et al. 2023. Comparative study of hydrodeoxygenation performance over Ni and Ni_2P catalysts for upgrading of lignin-derived phenolic compound. *Fuel* 331:125663

[65] Lu KL, Yin F, Wei XY, Li J, Li Z, et al. 2022. Promotional effect of metallic Co and Fe on Ni-based catalysts for p-cresol deoxygenation. *Fuel* 321:124033

[66] Yang F, Liu D, Zhao Y, Wang H, Han J, et al. 2018. Size dependence of vapor phase hydrodeoxygenation of m-cresol on Ni/SiO_2 catalysts. *ACS Catalysis* 8:1672–1682

[67] Yang F, Libretto NJ, Komarneni MR, Zhou W, Miller JT, et al. 2019. Enhancement of m-cresol hydrodeoxygenation selectivity on Ni catalysts by surface decoration of MoO_x species. *ACS Catalysis* 9:7791–7800

[68] Laurent E, Delmon B. 1994. Study of the hydrodeoxygenation of carbonyl, carboxylic and guaiacyl groups over sulfided CoMo/γ-Al_2O_3 and NiMo/γ-Al_2O_3 catalysts: I. catalytic reaction schemes. *Applied Catalysis A: General* 109:77–96

[69] Ruddy DA, Schaidle JA, Ferrell Iii JR, Wang J, Moens L, et al. 2014. Recent advances in heterogeneous catalysts for bio-oil upgrading via "ex-situ catalytic fast pyrolysis": catalyst development through the study of model compounds. *Green Chemistry* 16:454–490

[70] Radisavljevic B, Radenovic A, Brivio J, Giacometti V, Kis A. 2011. Single-layer MoS_2 transistors. *Nature Nanotechnology* 6:147–150

[71] Pan H, Zhang YW. 2012. Tuning the electronic and magnetic properties of MoS_2 nanoribbons by strain engineering. *The Journal of Physical Chemistry C* 116:11752–11757

[72] Lee TS, Esposito B, Donley MS, Zabinski JS, Tatarchuk BJ. 1996. Surface and buried-interfacial reactivity of iron and MoS_2: a study of laser-deposited materials. *Thin Solid Films* 286:282–288

[73] Gevert BS, Otterstedt JE, Massoth FE. 1987. Kinetics of the HDO of methyl-substituted phenols. *Applied Catalysis* 31:119–131

[74] Dolui K, Pemmaraju CD, Sanvito S. 2012. Electric field effects on armchair MoS_2 nanoribbons. *ACS Nano* 6:4823–4834

[75] Dominguez Garcia E, Chen J, Oliviero E, Oliviero L, Maugé F. 2020. New insight into the support effect on HDS catalysts: evidence for the role of Mo-support interaction on the MoS_2 slab morphology. *Applied Catalysis B: Environmental* 260:117975

[76] Diao X, Ji N. 2023. Rational design of MoS_2-based catalysts toward lignin hydrodeoxygenation: interplay of structure, catalysis, and stability. *Journal of Energy Chemistry* 77:601–631

[77] Lauritsen JV, Kibsgaard J, Olesen GH, Moses PG, Hinnemann B, et al. 2007. Location and coordination of promoter atoms in Co- and Ni-promoted MoS_2-based hydrotreating catalysts. *Journal of Catalysis* 249:220–233

[78] Daage M, Chianelli RR. 1994. Structure-function relations in molybdenum sulfide catalysts: The "rim-edge" model. *Journal of Catalysis* 149:414–427

[79] Delmon B, Froment GF. 1996. Remote control of catalytic sites by spillover species: a chemical reaction engineering approach. *Catalysis Reviews* 38:69–100

[80] Wang W, Zhang K, Qiao Z, Li L, Liu P, et al. 2014. Influence of surfactants on the synthesis of MoS_2 catalysts and their activities in the hydrodeoxygenation of 4-methylphenol. *Industrial & Engineering Chemistry Research* 53:10301–10309

[81] Gonçalves VOO, Brunet S, Richard F. 2016. Hydrodeoxygenation of cresols over Mo/Al_2O_3 and CoMo/Al_2O_3 sulfided catalysts. *Catalysis Letters* 146:1562–1573

[82] Fu J, Lym J, Zheng W, Alexopoulos K, Mironenko AV, et al. 2020. C–O bond activation using ultralow loading of noble metal catalysts on moderately reducible oxides. *Nature Catalysis* 3:446–453

[83] Chang JR, Chang SL, Lin TB. 1997. γ-Alumina-supported Pt catalysts for aromatics reduction: a structural investigation of sulfur poisoning catalyst deactivation. *Journal of Catalysis* 169:338–346

[84] Bui VN, Laurenti D, Afanasiev P, Geantet C. 2011. Hydrodeoxygenation of guaiacol with CoMo catalysts. *Part I: Promoting effect of cobalt on HDO selectivity and activity. Applied Catalysis B: Environmental* 101:239–245

[85] Song W, Zhou S, Hu S, Lai W, Lian Y, et al. 2019. Surface engineering of CoMoS nanosulfide for hydrodeoxygenation of lignin-derived phenols to arenes. *ACS Catalysis* 9:259–268

[86] Badawi M, Paul JF, Cristol S, Payen E, Romero Y, et al. 2011. Effect of water on the stability of Mo and CoMo hydrodeoxygenation catalysts: A combined experimental and DFT study. *Journal of Catalysis* 282:155–164

[87] Wang W, Tan S, Wu K, Zhu G, Liu Y, et al. 2018. Hydrodeoxygenation of p-cresol as a model compound for bio-oil on MoS_2: Effects of water and benzothiophene on the activity and structure of catalyst. *Fuel* 214:480–488

[88] Qu L, Jiang X, Zhang Z, Zhang XG, Song GY, et al. 2021. A review of hydrodeoxygenation of bio-oil: model compounds, catalysts, and equipment. *Green Chemistry* 23:9348–9376

[89] Lang M, Li H. 2022. Toward value-added arenes from lignin-derived phenolic compounds via catalytic hydrodeoxygenation. *ACS Sustainable Chemistry & Engineering* 10:13208–13243

[90] Lu J, Behtash S, Mamun O, Heyden A. 2015. Theoretical investigation of the reaction mechanism of the guaiacol hydrogenation over a Pt (111) catalyst. *ACS Catalysis* 5:2423–2435

[91] Zhang X, Tang W, Zhang Q, Li Y, Chen L, et al. 2018. Production of hydrocarbon fuels from heavy fraction of bio-oil through hydrodeoxygenative upgrading with Ru-based catalyst. *Fuel* 215:825–834

[92] Nie L, de Souza PM, Noronha FB, An W, Sooknoi T, et al. 2014. Selective conversion of m-cresol to toluene over bimetallic Ni-Fe catalysts. *Journal of Molecular Catalysis A: Chemical* 388:47–55

[93] Robinson A, Ferguson GA, Gallagher JR, Cheah S, Beckham GT, et al. 2016. Enhanced hydrodeoxygenation of m-Cresol over bimetallic Pt-Mo catalysts through an oxophilic metal-induced tautomerization pathway. *ACS Catalysis* 6:4356–4368

[94] Shi D, Arroyo-Ramírez L, Vohs JM. 2016. The use of bimetallics to control the selectivity for the upgrading of lignin-derived oxygenates: Reaction of anisole on Pt and PtZn catalysts. *Journal of Catalysis* 340:219–226

[95] Ballesteros-Plata D, Infantes-Molina A, Rodríguez-Cuadrado M, Rodríguez-Aguado E, Braos-García P, et al. 2017. Incorporation of molybdenum into Pd and Pt catalysts supported on commercial silica for hydrodeoxygenation reaction of dibenzofuran. *Applied Catalysis A: General* 547:86–95

[96] Yang F, Liu D, Wang H, Liu X, Han J, et al. 2017. Geometric and electronic effects of bimetallic Ni-Re catalysts for selective deoxygenation of m-cresol to toluene. *Journal of Catalysis* 349:84–97

[97] Liu X, An W, Turner CH, Resasco DE. 2018. Hydrodeoxygenation of m-cresol over bimetallic NiFe alloys: Kinetics and thermodynamics insight into reaction mechanism. *Journal of Catalysis* 359:272–286

[98] Hensley AJR, Zhang R, Wang Y, McEwen JS. 2013. Tailoring the adsorption of benzene on PdFe surfaces: a density functional theory study. *The Journal of Physical Chemistry C* 117:24317–24328

[99] Stevens MB, Anand M, Kreider ME, Price EK, Zeledón JZ, et al. 2022. New challenges in oxygen reduction catalysis: a consortium retrospective to inform future research. *Energy & Environmental Science* 15:3775–3794

[100] Gao Y, Yu J, Zhang B, Jin W, Zhang H. 2025. Enhanced targeted deoxygenation catalytic pyrolysis of lignin to aromatic hydrocarbons over oxygen vacancies Pt-MoOx/TiO2. *ChemCatChem* 17:e202401727

[101] Zhao C, Kou Y, Lemonidou AA, Li X, Lercher JA. 2009. Highly selective catalytic conversion of phenolic bio-oil to alkanes. *Angewandte Chemie-International Edition* 48:3987–3990

[102] Zhao C, Lercher JA. 2012. Upgrading pyrolysis oil over Ni/HZSM-5 by cascade reactions. *Angewandte Chemie-International Edition* 51:5935–5940

[103] XXia QN, Cuan Q, Liu XH, Gong XQ, Lu GZ, et al. 2014. Pd/$NbOPO_4$ multifunctional catalyst for the direct production of liquid alkanes from aldol adducts of furans. *Angewandte Chemie International Edition* 53:9755–9760

[104] Wang L, Zhang J, Yi X, Zheng A, Deng F, et al. 2015. Mesoporous ZSM-5 zeolite-supported Ru nanoparticles as highly efficient catalysts for upgrading phenolic biomolecules. *ACS Catalysis* 5:2727–2734

[105] Zhao C, He J, Lemonidou AA, Li X, Lercher JA. 2011. Aqueous-phase hydrodeoxygenation of bio-derived phenols to cycloalkanes. *Journal of Catalysis* 280:8–16

[106] Obenaus U, Dyballa M, Lang S, Scheibe M, Hunger M. 2015. Generation and properties of brønsted acid sites in bifunctional Rh-, Ir-, Pd-, and Pt- containing zeolites Y investigated by solid-state NMR spectroscopy. *The Journal of Physical Chemistry C* 119:15254–15262

[107] Cho HJ, Xu B. 2020. Enabling Selective Tandem Reactions via Catalyst Architecture Engineering. *Trends in Chemistry* 2:929–941

[108] Dai C, Zhang A, Song C, Guo X. 2018. Advances in the synthesis and catalysis of solid and hollow zeolite-encapsulated metal catalysts. *Advances in Catalysis* 63:75–115

[109] Shu R, Zhong Z, You H, Tian Z, Chen Y, et al. 2021. Hydrodeoxygenation of lignin-derived phenolic compounds over Ru/TiO_2-CeO_2 catalyst prepared by photochemical reduction method. *Journal of the Energy Institute* 99:1–8

[110] Olcese RN, Bettahar M, Petitjean D, Malaman B, Giovanella F, et al. 2012. Gas-phase hydrodeoxygenation of guaiacol over Fe/SiO_2 catalyst. *Applied Catalysis B: Environmental* 115:63–73

[111] Robinson AM, Hensley JE, Medlin JW. 2016. Bifunctional catalysts for upgrading of biomass-derived oxygenates: A review. *ACS Catalysis* 6:5026–5043

[112] Insyani R, Kim MK, Choi JW, Yoo CJ, Jin Suh D, et al. 2022. Selective hydrodeoxygenation of biomass pyrolysis oil and lignin-derived oxygenates to cyclic alcohols using the bimetallic NiFe core-shell supported on TiO_2. *Chemical Engineering Journal* 446:136578

[113] Wang Z, Wang CP, Mao SJ, Lu B, Chen Y, et al. 2022. Decoupling the electronic and geometric effects of Pt catalysts in selective hydrogenation reaction. *Nature Communications* 13:3561

[114] Luo WH, Cao WX, Bruijnincx PCA, Lin L, Wang A, et al. 2019. Zeolite-supported metal catalysts for selective hydrodeoxygenation of biomass-derived platform molecules. *Green Chemistry* 21:3744–3768

[115] Wu H, Song J, Xie C, Wu C, Chen C, Han B. 2018. Efficient and mild transfer hydrogenolytic cleavage of aromatic ether bonds in lignin-derived compounds over Ru/C. *ACS Sustainable Chemistry & Engineering* 6:2872–2877

[116] Guo M, Peng J, Yang Q, Li C. 2018. Highly active and selective RuPd bimetallic NPs for the cleavage of the diphenyl ether C–O bond. *ACS Catalysis* 8:11174–11183

[117] Zhang J, Wang B, Nikolla E, Medlin JW. 2017. Directing reaction pathways through controlled reactant binding at Pd-TiO_2 interfaces. *Angewandte Chemie International Edition* 56:6594–6598

[118] Niederberger M, Pinna N. 2009. Aqueous and nonaqueous sol-gel chemistry. In *Metal oxide nanoparticles in organic solvents: Synthesis, formation, assembly and application*. London: Springer London. pp. 7–18 doi: 10.1007/978-1-84882-671-7_2

[119] Fang H, Zheng J, Luo X, Du J, Roldan A, et al. 2017. Product tunable behavior of carbon nanotubes-supported Ni–Fe catalysts for guaiacol hydrodeoxygenation. *Applied Catalysis A: General* 529:20–31

[120] Mauriello F, Ariga-Miwa H, Paone E, Pietropaolo R, Takakusagi S, et al. 2020. Transfer hydrogenolysis of aromatic ethers promoted by the bimetallic Pd/Co catalyst. *Catalysis Today* 357:511–517

[121] Mortensen PM, Grunwaldt JD, Jensen PA, Jensen AD. 2013. Screening of catalysts for hydrodeoxygenation of phenol as a model compound for bio-oil. *ACS Catalysis* 3:1774–1785

[122] García-Fernández S, Gandarias I, Requies J, Güemez MB, Bennici S, et al. 2015. New approaches to the Pt/WO_x/Al_2O_3 catalytic system behavior for the selective glycerol hydrogenolysis to 1, 3-propanediol. *Journal of Catalysis* 323:65–75

[123] Sun J, Karim AM, Zhang H, Kovarik L, Li XS, et al. 2013. Carbon-supported bimetallic Pd-Fe catalysts for vapor-phase hydrodeoxygenation of guaiacol. *Journal of Catalysis* 306:47–57

[124] Zhang X, Tang W, Zhang Q, Wang T, Ma L. 2018. Hydrodeoxygenation of lignin-derived phenoic compounds to hydrocarbon fuel over supported Ni-based catalysts. *Applied Energy* 227:73–79

[125] Ambursa MM, Juan JC, Yahaya Y, Taufiq-Yap YH, Lin YC, et al. 2021. A review on catalytic hydrodeoxygenation of lignin to transportation fuels by using nickel-based catalysts. *Renewable & Sustainable Energy Reviews* 138:110667

[126] de Souza PM, Rabelo-Neto RC, Borges LEP, Jacobs G, Davis BH, et al. 2015. Effect of zirconia morphology on hydrodeoxygenation of phenol over Pd/ZrO_2. *ACS Catalysis* 5:7385–7398

[127] Ji N, Cheng S, Jia Z, Li H, Ri P, et al. 2022. Fabricating bifunctional Co-Al_2O_3@USY catalyst via in-situ growth method for mild hydrodeoxygenation of lignin to naphthenes. *ChemCatChem* 14:e202200274

[128] Liu X, Xu L, Xu G, Jia W, Ma Y, et al. 2016. Selective hydrodeoxygenation of lignin-derived phenols to cyclohexanols or cyclohexanes over magnetic CoN_x@NC catalysts under mild conditions. *ACS Catalysis* 6:7611–7620

[129] Han GH, Lee MW, Park S, Kim HJ, Ahn JP, et al. 2019. Revealing the factors determining the selectivity of guaiacol HDO reaction pathways using ZrP-supported Co and Ni catalysts. *Journal of Catalysis* 377:343–357

[130] Liu X, Jia W, Xu G, Zhang Y, Fu Y. 2017. Selective Hydrodeoxygenation of Lignin-Derived Phenols to Cyclohexanols over Co-Based Catalysts. *ACS Sustainable Chemistry & Engineering* 5:8594–8601

[131] Jiang L, Guo H, Li C, Zhou P, Zhang Z. 2019. Selective cleavage of lignin and lignin model compounds without external hydrogen, catalyzed by heterogeneous nickel catalysts. *Chemical Science* 10:4458–4468

[132] Echeandia S, Pawelec B, Barrio VL, Arias PL, Cambra JF, et al. 2014. Enhancement of phenol hydrodeoxygenation over Pd catalysts supported on mixed HY zeolite and Al_2O_3. *An approach to O-removal from bio-oils. Fuel* 117:1061–1073

[133] He S, Li C, Chen H, Su D, Zhang B, et al. 2013. A surface defect-promoted Ni nanocatalyst with simultaneously enhanced activity and stability. *Chemistry of Materials* 25:1040–1046

[134] McDonough WF, Sun Ss. 1995. The composition of the Earth. *Chemical Geology* 120:223–253

[135] Sun L, Zhang X, Chen L, Zhao B, Yang S, et al. 2016. Comparision of catalytic fast pyrolysis of biomass to aromatic hydrocarbons over ZSM-5 and Fe/ZSM-5 catalysts. *Journal of Analytical and Applied Pyrolysis* 121:342–346

[136] Hong Y, Hensley A, McEwen JS, Wang Y. 2016. Perspective on catalytic hydrodeoxygenation of biomass pyrolysis oils: essential roles of Fe-Based catalysts. *Catalysis Letters* 146:1621–1633

[137] Olcese R, Bettahar MM, Malaman B, Ghanbaja J, Tibavizco L, et al. 2013. Gas-phase hydrodeoxygenation of guaiacol over iron-based catalysts. Effect of gases composition, iron load and supports (silica and activated carbon). *Applied Catalysis B: Environmental* 129:528–538

[138] Olcese RN, Lardier G, Bettahar M, Ghanbaja J, Fontana S, et al. 2013. Aromatic chemicals by iron-catalyzed hydrotreatment of lignin pyrolysis vapor. *ChemSusChem* 6:1490–1499

[139] Tan Q, Wang G, Long A, Dinse A, Buda C, et al. 2017. Mechanistic analysis of the role of metal oxophilicity in the hydrodeoxygenation of anisole. *Journal of Catalysis* 347:102–115

[140] Tan H, Rong S, Zhao R, Cui H, Zhang NN, et al. 2022. Targeted conversion of model phenolics in pyrolysis bio-oils to arenes via hydrodeoxygenation over MoO_x/BaO@SBA-15 catalyst. *Chemical Engineering Journal* 438:135577

[141] Shetty M, Murugappan K, Green WH, Román-Leshkov Y. 2017. Structural properties and reactivity trends of molybdenum oxide catalysts supported on zirconia for the hydrodeoxygenation of anisole. *ACS Sustainable Chemistry & Engineering* 5:5293–5301

[142] Kasiraju S, Grabow LC. 2018. Learning from the past: Are catalyst design principles transferrable between hydrodesulfurization and deoxygenation? *AIChE Journal* 64:3121–3133

[143] Ressler T, Jentoft RE, Wienold J, Günter MM, Timpe O. 2000. In situ XAS and XRD studies on the formation of Mo suboxides during reduction of MoO_3. *The Journal of Physical Chemistry B* 104:6360–6370

[144] Talebkeikhah F, Sun S, Luterbacher JS. 2023. Sinter-resistant nickel catalyst for lignin hydrogenolysis achieved by liquid phase atomic layer deposition of alumina. *Advanced Energy Materials* 13:2203377

[145] Vo TK, Quang DT, Kim J. 2022. Spray pyrolysis-derived MoO_3@Al_2O_3@TiO_2 core-shell structures with enhanced hydrodeoxygenation performance. *Catalysis Communications* 169:106478

[146] Moon JS, Lee YK. 2015. Support effects of Ni_2P catalysts on the hydrodeoxygenation of guaiacol: in situ XAFS studies. *Topics in Catalysis* 58:211–218

[147] Wei X, Xue X, Wu L, Yu H, Liang J, et al. 2020. High-grade bio-oil produced from coconut shell: a comparative study of microwave reactor and core-shell catalyst. *Energy* 212:118692

[148] Wang C, Ou J, Zhang T, Xia S, Kang S, et al. 2023. Sustainable aromatic production from catalytic pyrolysis of lignin mediated by a novel solid lewis acid catalyst. *Fuel* 348:128513

[149] Crucho CIC. 2024. Silica coatings: From nanostructures to biological entities. *Applied Materials Today* 38:102179

[150] Duan L, Wang C, Zhang W, Ma B, Deng Y, et al. 2021. Interfacial assembly and applications of functional mesoporous materials. *Chemical Reviews* 121:14349–14429

[151] Jiang W, Xiao J, Gao X, An X, Leng Y, et al. 2021. In situ fabrication of hollow silica confined defective molybdenum oxide for enhanced catalytic oxidative desulfurization of diesel fuels. *Fuel* 305:121470

[152] Wang W, Zhang H, Zhou F, Xiang Z, Zhu W, et al. 2023. Al-doped core-shell-structured Ni@mesoporous silica for highly selective hydrodeoxygenation of lignin-derived aldehydes. *ACS Applied Materials & Interfaces* 15:33654–33664

[153] Jamsaz A, Pham-Ngoc N, Wang M, Jeong DH, Oh ES, et al. 2023. Synergistic effect of macroporosity and crystallinity on catalyst deactivation behavior over macroporous Ni/CexZr$_{1-x}$O$_2$-Al$_2$O$_3$ for dry reforming of methane. *Chemical Engineering Journal* 476:146821

[154] Liang D, Wang Y, Wang Y, Chen M, Xie X, et al. 2024. Dry reforming of methane for syngas production over noble metals modified M-Ni@S-1 catalysts (M=Pt, Pd, Ru, Au). *International Journal of Hydrogen Energy* 51:1002–1015

[155] Xue S, Luo Zy, Wang Wb, Li S, Sun H, et al. 2020. Preparation of aromatics from catalytic pyrolysis of enzymatic lignin over double-layer metal supported core-shell catalyst. *Journal of Analytical and Applied Pyrolysis* 150:104884